

AN ABSTRACT OF THE THESIS OF

Yin - Shing Chong for the degree of Master of Science in Mechanical Engineering presented on April 21, 1995.

Title: A Numerical and Experimental Investigation of Rectangular Abrasive Jets for Drilling Operations.

Redacted for Privacy

Abstract approved:_____

 Dwight J. Bushnell _____

This thesis presents the preliminary experimental results obtained on specially designed abrasive rectangular nozzles for micro - drilling. Four different sizes of rectangular nozzles were used for drilling. All experiments were conducted with an inlet nozzle pressure of 80 psi with Al_2O_3 used as the abrasive particles impacting on a flat 2 mm thick tool steel plate.

Experimental observations during the drilling process revealed deeper penetration occurring at the ends of the rectangular crater, while less penetration occurred at the center of the crater. The particle flowrate was found to be dependent on both the orifice and the inlet nozzle pressure. From the drilling experiments the results indicated that the nozzle to substrate (NTS) distance, pressure and mixture ratio are the important parameters affecting the drilling rate.

A commercial numerical code, FLUENT was used to model the two phase jet. FLUENT was verified by comparing the pressure at impact location to numerical results for a single phase flow. In the two phase flow, although verification was not attempted, experimental observation found that FLUENT was able to predict the

erosions that were found in the actual nozzle and can be used as a tool for designing a nozzle.

A Numerical and Experimental Investigation of
Rectangular Abrasive Jets for Drilling Operations

by

Yin-Shing, Chong

A THESIS

submitted to

Oregon State University

in partial fulfillment of
the requirements for the
degree of

Master of Science

Completed April 21, 1995
Commencement June 1995

Master of Science thesis of Yin - Shing, Chong presented on April 21, 1995

APPROVED:

Redacted for Privacy

Major Professor, representing Mechanical Engineering

Redacted for Privacy

Acting Head of Department of Mechanical Engineering

Redacted for Privacy

Dean of Graduate School

I understand that my thesis will become part of the permanent collection of Oregon State University libraries. My signature below authorizes release of my thesis to any reader upon request.

Redacted for Privacy

Yin^v-Shing, Chong, Author

ACKNOWLEDGEMENT

I would like to express my heartfelt gratitude to Dr. Dwight Bushnell; first for giving me the opportunity to work on an advanced degree on this project, and second for the time, patience and advice given throughout this project. His help and guidance was invaluable to the completion for this project.

I also would like to thank Hewlett Packard's IJBU unit for funding this project and providing facilities and equipment. This gratitude is also extended to the Drill Team in Hewlett Packard for their time and invaluable assistance, without their help the completion of this project would not be possible.

TABLE OF CONTENTS

	<u>Page</u>
INTRODUCTION	1
LITERATURE REVIEW	5
PROJECT OBJECTIVES AND APPROACH	9
EXPERIMENTS	14
Experiment I	14
Experiment II	20
Experiment III	23
NUMERICAL EXPERIMENT	26
RESULTS	31
Experiment I	31
Experiment II	33
<u>Time Effect</u>	33
<u>Effect of Pressure</u>	41
Experiment III	47
<u>Evaluation of Numerical Method</u>	47
<u>Validation of Two Phase Flow</u>	67
CONCLUSIONS	71
BIBLIOGRAPHY	74

LIST OF FIGURES

<u>Figure</u>		<u>Page</u>
1.	Surface Impingement of Jet	3
2.	Diagram of a Free Jet	13
3.	A Simplified Layout of Experiment I	14
4.	A Simplified Layout of Experiment II	21
5.	Nozzle Assembly	23
6.	A Simplified Layout of Experiment III	25
7.	Pressure and Voltage Relationship (SENSYM Sensor)	25
8.	Position of Injection Points	28
9.	Geometrical Meshing of Nozzle	29
10.	Selected Slices of Model in Computational Domain	30
11.	Sand Flowrate for All Nozzles at Inlet Pressure of 80 psi	32
12.	Sand Flowrate with Respect to Nozzle Inlet Pressure	32
13a -13d.	A Least Square Fit of the Time Effect on Penetration Depth for All Nozzles and at All NTS Distances at an Inlet Pressure of 80 psi ...	35
14a -14d.	Time Effect on Length for All Nozzles and at All NTS Distances at an Inlet Pressure of 80 psi	36
15a - 15d.	Time Effect on Width for All Nozzles and at All NTS Distances at an Inlet Pressure of 80 psi	37
16.	Structure of Two Phase Jet	38
17a.	Laser Scan of Crater Across the Length	38
17b.	Laser Scan of Multiple Craters Across the Width	39
18.	Energy Distribution and Resulting Width and Length	41

List of Figures, Continued

19a - 19d.	2nd Order Polynomial Fit of Pressure Effect on Penetration Depth for All Nozzles and at All Distances with Dwelling Time of 10 Seconds	44
20a - 20d.	Pressure Effect on Length for All Nozzles and at All NTS Distances with Dwelling Time of 10 Seconds	45
21a - 21d.	Pressure Effect on Width for All Nozzles and at All NTS Distances with Dwelling Time of 10 Seconds	46
22.	Velocity Contours of Single Phase Gas Jet for Aspect Ratio 10 Nozzle at NTS 40	48
23.	Velocity Contours of Single Phase Gas Jet for Aspect Ratio 10 Nozzle at NTS 60	48
24.	Velocity Contours of Single Phase Gas Jet for Aspect Ratio 10 Nozzle at NTS 80	49
25.	Velocity Contours of Single Phase Gas Jet for Aspect Ratio 10 Nozzle at NTS 100	49
26.	Velocity Contours of Single Phase Gas Jet for Aspect Ratio 20 Nozzle at NTS 40	50
27.	Velocity Contours of Single Phase Gas Jet for Aspect Ratio 20 Nozzle at NTS 60	50
28.	Velocity Contours of Single Phase Gas Jet for Aspect Ratio 20 Nozzle at NTS 80	51
29.	Velocity Contours of Single Phase Gas Jet for Aspect Ratio 20 Nozzle at NTS 100	51
30.	Velocity Contours of Single Phase Gas Jet for Aspect Ratio 30 Nozzle at NTS 40	52
31.	Velocity Contours of Single Phase Gas Jet for Aspect Ratio 30 Nozzle at NTS 60	52
32.	Velocity Contours of Single Phase Gas Jet for Aspect Ratio 30 Nozzle at NTS 80	53

List of Figures, Continued

33.	Velocity Contours of Single Phase Gas Jet for Aspect Ratio 30 Nozzle at NTS 100	53
34.	Velocity Contours of Single Phase Gas Jet for Aspect Ratio 40 Nozzle at NTS 40	54
35.	Velocity Contours of Single Phase Gas Jet for Aspect Ratio 40 Nozzle at NTS 60	54
36.	Velocity Contours of Single Phase Gas Jet for Aspect Ratio 40 Nozzle at NTS 80	55
37.	Velocity Contours of Single Phase Gas Jet for Aspect Ratio 40 Nozzle at NTS 100	55
38.	Velocity Contours of Two Phase Flow Jet for Aspect Ratio 10 Nozzle at NTS 100	56
39.	Velocity Contours of Two Phase Flow Jet for Aspect Ratio 20 Nozzle at NTS 100	56
40.	Velocity Contours of Two Phase Flow Jet for Aspect Ratio 30 Nozzle at NTS 100	57
41.	Velocity Contours of Two Phase Flow Jet for Aspect Ratio 40 Nozzle at NTS 100	57
42a - 42d.	Total Pressure Comparison for Aspect Ratio 10 Nozzle	60
43a - 43d.	Total Pressure Comparison for Aspect Ratio 20 Nozzle	61
44a - 44d.	Total Pressure Comparison for Aspect Ratio 30 Nozzle	62
45a - 45d.	Total Pressure Comparison for Aspect Ratio 40 Nozzle	63
46a - 46d.	Total Pressure Comparison for Aspect Ration 10 Nozzle with 0.006 inch Pitot Tube	64
47.	Geometrical Meshing of Model with Tube at the Plate to Simulate a Pitot Tube	65
48.	Pressure Plots Showing the Effect of Tube by Numerical Method	65

List of Figures, Continued

49a - 49b	Verification with " Schlichting Formula "	66
50a.	Photograph Showing Erosion at Entrance of Nozzle	68
50b.	Photograph Showing Erosion at Wall of Nozzle	68
51.	Particle Tracks Showing the Points of Impacts at Nozzle Entrance and Wall	51
52a - 52b.	Particle Impact Points on Steel Plate for Aspect Ratios 10 and 40 Nozzle at NTS 100 mils	70
53a - 53b	Normalized Momentum and Depth Comparison along Length of slot	71

LIST OF TABLES

<u>Table</u>		<u>Page</u>
1.	An Example of Particles Size and Mass Distribution	18
2.	An Example of Data Recast in Rosin - Rammler Format	19
3.	Pressure Boundary, Sand and Air Flowrate	20
4.	Orifice Size of Nozzles	22
5.	Materials Properties	27
6.	Air Flowrate Comparison	58

A Numerical and Experimental Investigation of Rectangular Abrasive Jets for Drilling Operations

INTRODUCTION

Abrasive jet machining (AJM), until recently, was used mainly in deburring, cleaning, frosting, and marking on hard surfaces. Its limited usage was due mainly to the bulky equipment associated with AJM, and also because the variables to control the sand flow in the equipment are so numerous, that it requires frequent tuning and adjustment to get the equipment to work correctly.

With the advances made in controlling sand flow, abrasive jet machining has again generated great interest. This is especially true with the use of advanced materials (e.g. ceramics, ceramic composites) for use in extreme operating conditions for instance in high operating temperatures. Common methods of machining these materials are abrasive grinding, chemical, electro-chemical, ultrasonic and EDM machining. The traditional machining methods, where there is tool to part contact, like drilling or milling have proven to be problematic in machining such hard materials without compromising the parameters that are so interdependent between the machined parts and productivity.

With the advent of clean and high energy forms of material removal techniques like lasers, water jets, and abrasive jet machining a new dimension for machining hard and brittle materials has opened. AJM has several advantages over the traditional methods and also other new machining methods. The most significant advantage of AJM is that there is minimum of thermal distortion induced onto the part as is the

case with laser or plasma cutting. Also in the AJM process, subsurface damage by tool to part contact is greatly minimized and the cost AJM compared to other non-traditional machining methods is considerably less.

In abrasive jet machining, material is removed by the impact of fine particles impinging onto the material at high velocity. The angle of impact where maximum erosion occurs is very dependent on the type of materials on which the particles are impinging. For brittle materials, it was found that, an impact angle perpendicular to the impacted surface produced maximum erosion (Finnie 1960). While in ductile material, the effective angle was determined to be between 20 - 30 degrees from the surface of the material.

In the study of AJM, there are two forms of erosion rates. In applications where AJM is used for polishing, deburring and other finishing operations the weight/volume of the eroded material is important. In cases like drilling or other cutting operations the penetration depth (erosion depth) is more relevant. For this project, the interest is in the application of AJM for creating a rectangular hole in hard and brittle materials. As such, the mechanism of material removal by AJM is of interest and the penetration rate will be used as a basis of measurement.

The main disadvantage of abrasive jet machining is that it is hard to predict the hole size produced by the nozzle. In designing the nozzle of an abrasive jet for drilling there is no clear or systematic approach used which guarantees that the orifice of the nozzle will produce a jet that will drill a hole to the right specification. Many a time, a nozzle was designed slightly smaller than the specified slot size, by adjusting

some independent variables like standoff distance and the line pressure in order to achieve the slot specification.

When the abrasive jet is brought near to the surface to be cut, the flow of the free jet is disrupted. At the impinging zone or the stagnation zone, (see figure 1) the flow is decelerated normally. Then the flow is redirected to flow along the surface of the material thus forming a wall jet. The abrasive particles which have momentum imparted to it by the carrier fluid will impinge on to the material and finally be carried out by the wall jet. Some of the particles are reflected upstream until they are decelerated by the gas flow and are again carried back in the main flow direction and eventually escape to the atmosphere.

It is the interest of this project to investigate how the flow of the jet is

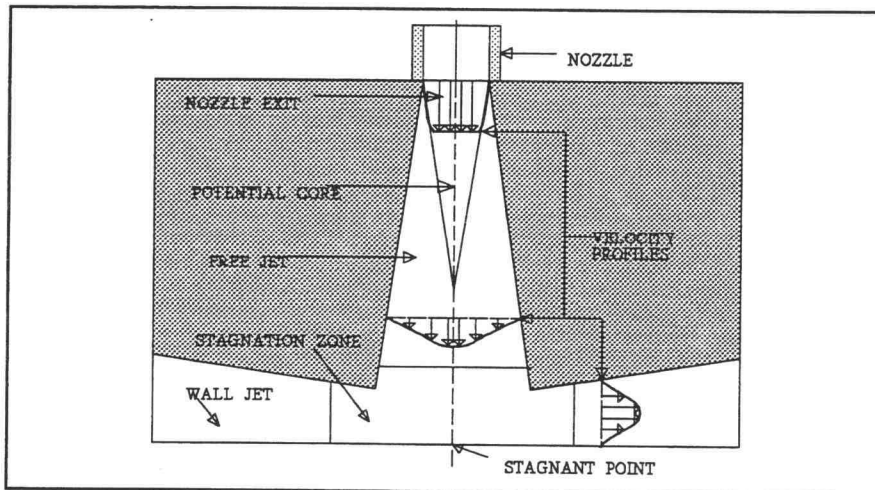


Figure 1: Surface Impingement of Jet

affected when the impinging distance (standoff distance) is varied. When AJM is used for drilling purposes, the consistency of the hole size becomes very important. Thus, in the study of the parameters that influence the jet and the hole size; the stand-off distance, operating pressure, particle loading and sizes become critical to the abrasive jet. There is a need also to understand if the relationship between the nozzle size and the influencing parameters will help in controlling the size of the hole being drilled and eventually the design of the nozzle.

LITERATURE REVIEW

With the advent of advanced materials being used in the electronic industries, the abrasive air jet has been found to be useful in manufacturing processes. In abrasive jet machining (AJM), the material is removed by erosion induced by fine abrasive particles impinging at high velocity onto the material.

Finnie's (1960) studies on the mechanism of material removal by impacting particles demonstrated that the volume of the material removed by an impacting particle carried in an air stream was influenced by parameters such as: impingement angle, particle velocity and size and nature of the carrier fluid. Sheldon (1966) and Bitter (1963) also indicated that the angle of impact of the particles also influenced the erosion rate. The erosion rate for brittle materials was a maximum when the impingement angle was at 90 degrees. Ductile materials demonstrated maximum erosion when the impingement angle was between 20 and 30 degrees to the surface of the material.

Fisher and Davis (1949) performed work on fly-ash erosion and found that material erosion rates increased with the increase of both the impact velocity and stand-off distance. Smeltzer (1970) revealed that erosion rate per particle flux decreased when the particle concentration increased. This phenomenon was also observed by Tilly (1979) who described a typical reduction of erosion rate of 50% for a fortyfold increase in particle concentration. Ingulli (1967), Panddy (1977) and Bhattacharya (1977) made a more intensive study on the effects of abrasive flowrate

and standoff distance on the erosion rate. They found that the rate of the material removed first increased with increase in abrasive flowrate and standoff distance and then decreased with further increase in those parameters.

Particles had a threshold diameter where the aerodynamic drag was the greatest in a two phase flow as determined by Balanin, Lashkov and Trakhov (1981). Their experiment revealed that when the mass average particle diameter was less than thirty micrometers, the solids lagged only slightly behind the gas, and the flow behaved as a quasigas. When the diameter was greater than thirty micrometers, the particles lag became very significant and the effect of the particle phase in the jet decreases.

The uses of abrasive jet machining is found mostly in deburring, polishing and other surface finishing operations. In such applications, the material removal rate is evaluated in terms of the weight of the material removal per unit time. But as for the case of a drilling operation, measuring the eroded depth is more relevant than the amount of material removed. Verma and Lal (1984) performed an experiment of abrasive air jet emerging from a round nozzle based on the experimental method performed by Ingulli, Panddy and Bhattacharya.

In the Verma and Lal experiment, it was found that the penetration rate and the material removal rate first increased with an increase in stand-off distance and then decreased giving an optimum. The peak of both erosions (penetration rate and volumetric material removal rate) occurred at different standoff distances. The experiment also found that the penetration depth increased with increase in mixture ratio and the standoff distance corresponding to the optimum penetration rate also

increased with mixture ratio.

Sommerfeld (1991), did work on the expansion of a gas and particle mixture in supersonic jet flow. He found that the mach disk moves downstream and eventually disappeared as the mass loading of particles was increased. He also showed that the different sizes and mass loading of particles also affect the spread of the jet. In Sommerfeld's experiment, very small particles were found to follow the gas flow easily, which resulted in an equilibrium flow. The size distribution of the particles for different radial locations of the jet was explored. It was discovered that a fraction of small particles was found to be away from the jet axis, whereas the larger particles flowed mainly in the jet core. The velocity gained by the particles was found to be only forty percent of the carrier fluid and also that the particles velocity decreases with increase of particle loading and particle diameter.

Literature for abrasive air jets from a rectangular nozzle was scarce. Most of the work done for rectangular jets was of single phase and studied mainly in the interest of engineering applications such as thrust augmenting ejectors for VTOL/STOL aircraft or in paper drying industries. Forthmann (1936) was probably the first to conduct an extensive research on the single phase rectangular jet. The author found that by plotting the ratio of the distance between the jet axis and the point where the velocity equaled half the axial velocity there was a similarity of the jet characteristic with round jets. Recent work by Krothapalli, Baganoff and Karamcheti (1979) found the flow field of a rectangular jet to be characterized by the presence of three distinct regions which were referred to as a potential core region, a two

dimensional type region and an axisymmetric type region.

Marsters (1979, 1980) determined that the shape of a single phase rectangular jet stream depended on the shape of the nozzle upstream. The jet from a rectangular orifice plate exhibited a saddle profile, while a nozzle which had a smooth contraction upstream of the jet exhibited a flat profile both lengthwise and widthwise. The jet discharging from a nozzle that had a long upstream channel presented a thick boundary layer i.e. a fully developed flow. It was also observed that the velocity profile of the jet when looking across the length of the nozzle orifice is very steep along the side and the front or face of the profile is flat like a plug flow or a saddle like profile. The velocity profile when observed across the width, on the other hand, exhibits a bell shape profile. Both velocity profiles however flatten as the jet is spreading out due to air friction away from the nozzle exit.

PROJECT OBJECTIVES AND APPROACH

The main objective of this project is to investigate the characteristics of an abrasive rectangular jet impinging on a plate for use in drilling operations.

Investigations are both experimental and numerical.

To date, the studies on abrasive jet machining are either done by experimentation or computer modeling. In previous studies of AJM by computer modeling, momentum exchange between the particles and the driving fluid was verified. In addition, the flight of the particles from the nozzle exit to the point of impact was also simulated. The simulations were for subsonic flow and from a round nozzle.

Most of the study done on AJM thus far was by experimentation. This seems to be the most common method adopted by many researchers. The reason for this undertaking is due to the many variables that are involved in AJM. Unfortunately this type of experimentation can be very expensive. Reasons for this high cost are due to the abrasive nature of the jet in AJM and also the time to qualify a nozzle suitable for drilling. The material used to make the nozzle must also be very wear resistant and hard. Experience has shown that the cost of the nozzle is proportional to the hardness of the material, and require tolerances. Thus for a simple study of AJM, many nozzles have to be manufactured before one is deemed as suitable for drilling.

The long range objective of this project is to determine if a CFD software package, available in the market place, can be incorporated in studying of AJM

without having to resort to expensive experimentation. Equally important is to determine if the CFD package can assist in the preliminary stage of nozzle design, thus cutting the lead time of producing and optimizing a nozzle. It is also an objective of this project to determine if the data collected from experiments can provide a better understanding of rectangular slot generation by AJM and also be used to assist nozzle designers to predict the size of the hole created by the nozzle. The direction that this preliminary study undertakes was of two steps.

I: As this was the preliminary stage of the experiment in the study of abrasive jet machining of a rectangular nozzle, simple experiments were first conducted for four nozzles of aspect ratio 10, 20, 30 and 40. In the experiment, the abrasive jet was impinged onto a tool steel plate which was placed at a distance of 40, 60, 80 and 100 thousandth of an inch (mils) from the outlet of the nozzle.

Two experiments were conducted to look at the

- i . the time effect
- ii . the pressure effect

In the time effect experiments, the dwelling time of the jet onto the steel plate was from 5 seconds to 90 seconds. The input pressure at the inlet for all nozzles was held constant at 80 psi.

In the studies of pressure effect, slots were created by varying the operating pressure from 30 to 140 psi for all the nozzles. The drilling time was held constant at 10 seconds for the experiments.

The results of the penetration depth, length and width growth for both experiments were plotted and measurement of the profile of the rectangular crater will also be presented.

II: An existing computational fluid dynamics software (FLUENT) was evaluated for applicability as a tool to model the abrasive rectangular jet. Numerical simulations were performed for single and two phase flow. The results from the numerical simulations were then be compared with the experimental results to verify the computer model.

Verification of the computer software can be made by comparing the stagnation pressures measured during the experiment and the numerical simulation. The stagnation pressure is being used as a criteria of comparison because erosion of the plate is caused by the impact force of the jet. This impact force can be measured by measuring the stagnation pressure at the point of impact. This theory was validated by Kinoshita (1976). Kinoshita showed that for a high speed (sonic) jet that impinges on a wall, the impact force of the jet can be estimated by the pressure recovery after the detached or normal wave.

Verifications of the numerical method for the single phase flow without resorting to experiments can be performed by using "the law of 3/2" or the "Schlichting formula". This law is applicable because the profile of the dimensionless velocity (relative to the velocity along the jet) in the cross sections of a jet is universal and its form does not depend upon the parameters of the moving fluid. It can be used for various conditions of jet discharge from a nozzle including

nonisothermal jets in an external streams, supersonic submerged heated and cooled jets, supersonic under off-design discharge conditions.

In treating the velocity profile for the initial region of the jet , the formula stated below is used

$$\Delta \bar{U} = \frac{(U_1 - U)}{(U_1 - U_2)} = f(\eta) = (1 - \eta^{1.5})^2 \quad (1)$$

where

$$\eta = \frac{(y - y_2)}{(y_1 - y_2)} = \frac{(y - y_2)}{b} \quad (2)$$

and $b = Y_1 - Y_2$

y_1 is the ordinate of the internal boundary of the turbulent border layer

y_2 is the ordinate of the external boundary of the turbulent border layer

U_1 is the velocity at the internal boundary of the turbulent border layer

U_2 is the velocity at the external boundary of the turbulent border layer

Equations 3 and 4 below are used in the main region.

$$\Delta \bar{U} = \frac{(U - U_c)}{(U_o - U_c)} = \frac{\Delta U}{\Delta U_o} = f(\xi) = (1 - \xi^{1.5})^2 \quad (3)$$

where

$$\xi = \frac{Y}{2.27Y_h}$$

(4)

and Y represents the ordinate of points which correspond to arbitrary value of dimensionless velocity
 Y_h represents the ordinate of points which correspond the velocity which is one - half of the axial velocity (U_o), see figure 2
 U_o is the velocity at the boundary.

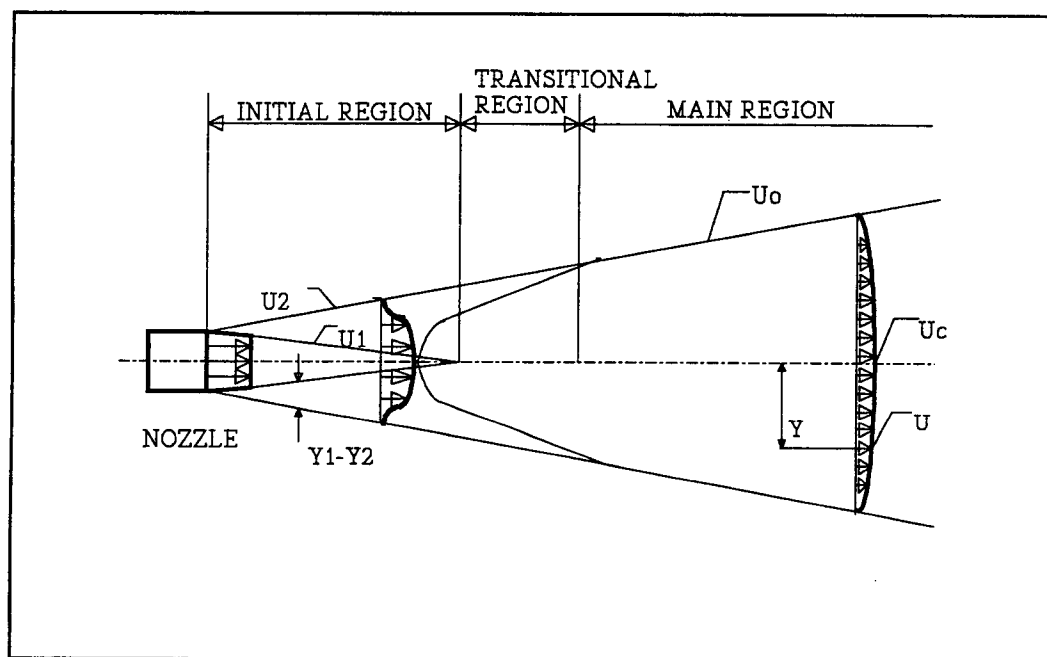


Figure 2: Diagram of a Free Jet

EXPERIMENTS

The experiments for this project were divided into three parts. The first experiment was conducted on all the nozzles to establish the boundary conditions needed for numerical modeling. The second part was to determine the effect of the influencing parameters such as the standoff distance, operating pressure and particle loading and sizes on the abrasive jet and the erosion rate. The third part was the computer model verification studies.

EXPERIMENT I

The boundary conditions needed for numerical simulation were:

- i. Flowrate of air and abrasive particles
- ii. Size distribution of abrasive particles
- iii. Inlet and outlet pressure of the nozzles

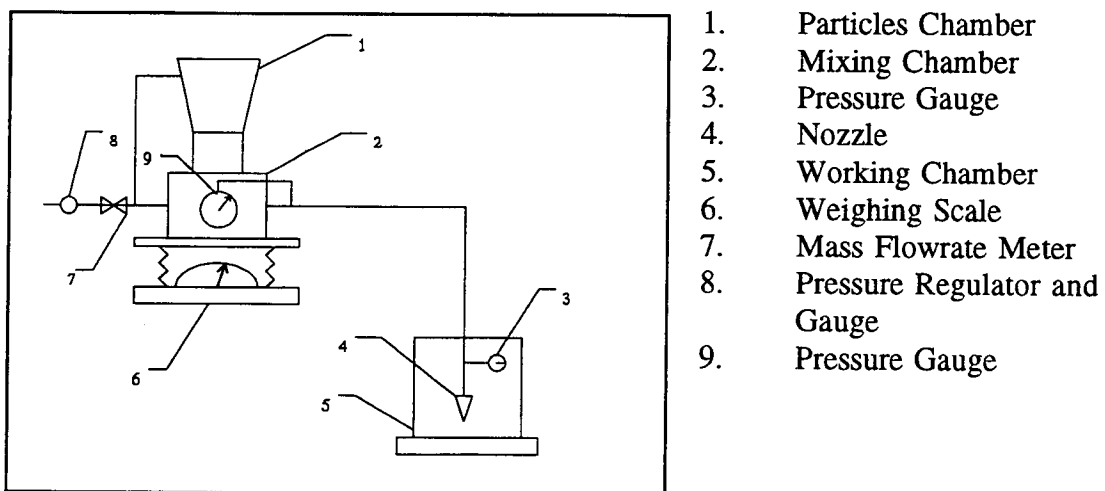


Figure 3: A Simplified Layout of Experiment I

The nozzles used for the experiments were made of carbide steel and finely ground aluminum oxide was used as the abrasive particles. An Omega Flowrate meter and its adapter, FPW-D15, were used for measuring the air flowrate. The output of the flowrate meter was displayed and recorded through a Fluke 97 scopemeter. Two , USG, 0 - 200 psig with 1 psig sub-division pressure gauges were also used to measure pressure losses in the line and a METTLER model pm34-k Delta Range weighing machine, capable of measuring to a tenth of a gram, was used to weigh the amount of abrasive particles used.

A simplified schematic of the apparatus is shown in Figure 3. Air which was dried, compressed and filtered flows through the mixing chamber. Fine grained abrasive powder contained in the main abrasive chamber flows down into the mixing chamber was carried by the air to the nozzle and finally to the working chamber. The pressure in the main abrasive chamber was kept at the same pressure as the incoming air. The flow of the aluminum oxide from the particles chamber into the air stream was partly gravity assisted and partly assisted by a shuttle valve placed before the outlet of the abrasive particle chamber. The shuttle valve oscillating back and forth at 60 Hz, caused pressure fluctuations in the line. These pressure fluctuations fluidized the particles near the exit of the chamber which allow the abrasive particles to flow into the incoming air stream easily.

The pressure and air flowrate in the system was maintained by a regulator. A pressure gauge, connected at the regulator, displayed the air pressure of the mixing and abrasive chamber. Another pressure gauge at the nozzle inlet showed the pressure

at that location. At the mixing chamber inlet, the Omega mass flowrate meter was connected to measure the air flowrate.

The assembly of the abrasive powder chamber, mixing chamber and the measuring devices were placed on the METTLER weighing scale. This weighing scale was used to determine the amount of abrasive particle consumed. The abrasive particle consumption rate was found by letting the air and abrasive particles mixture discharge at the nozzle for approximately an hour. Readings were then taken every five minutes during this time to obtain an average consumption rate.

The Omega mass flowrate meter measured the air flowrate in standard liters per minute at 75° F. The range of the meter was from 0 to 5 V, corresponding to 0 and 200 liters per minute respectively. The conversion from standard liter per minute to operating conditions could be found with an appropriate equation of state. The final conversion equation is shown below.

$$\dot{V}_{op} = \frac{P_{atm}}{(P_{atm} + P_{op})} \dot{V}_{measured}$$

(5)

Where \dot{V}_{op}	is the volumetric flowrate of air at operating condition
$\dot{V}_{measured}$	is the measured flowrate of air
P_{op}	is the operating pressure
P_{atm}	is the atmospheric pressure

Since the abrasive particles were ground, a Rosin - Rammler approach was used to determine the size distribution of the sand. The Rosin - Rammler function (eqn 6) is based on the assumption that an exponential relationship exists between the abrasive particles diameter D and mass fraction of particles with diameter greater than the particles diameter D .

$$M_D = \exp\left(-\left(\frac{D}{\bar{D}}\right)^n\right)$$

(6)

where M_D is the mass fraction
 D is the diameter of particles
 \bar{D} is the mean diameter of particles and
 n is the spread parameter

The parameters \bar{D} , M_D and n must be found. From the aluminum oxide supplier, M_D and D were taken from the abrasive particles size distribution. As an example, let's assume that the particles size distribution as obtained from the supplier is listed below.

Table 1: An Example of Particles Size and Mass Distribution

Diameter Range (μm)	Mass Fraction in the Range
0 - 50	0.05
50 - 70	0.10
70 - 120	0.35
120 - 160	0.30
160 - 200	0.15
200 - 230	0.05

The distribution was then recast into Rosin - Rammler format as shown in table 2.

The value of \bar{D} was obtained by equating M_D to -1 which was 0.368. i.e. D and \bar{D}

were set equal. Then by plotting a graph using table 2, the value of D could be

approximated. The value of the parameters were substituted into equation 2 and n

was then found. This was repeated several times to obtain an average value. By the

same process and with the actual supplier data, the mean diameter was found to be 30

microns and the spread parameter for the abrasive powder was 2.5 microns.

Table 2: An Example of Data Recast in Rosin - Rammler Format

Diameter, D (μm)	Mass Fraction with Diameter Greater than D, M_D
50	0.95
70	0.85
120	0.50
160	0.20
200	0.05
230	0.00

In this experiment it was decided to maintain the pressure at the nozzle inlet at 80 psi. It was found that to maintain 80 psi for each nozzle, the upstream pressure at the regulator had to be set differently for each nozzle. This was due to the pressure losses for different aspect ratio nozzles. Nozzle of aspect ratio 10 was found to have

the greatest losses and aspect ratio 40 nozzle had the least. The results of the experiment are tabulated below.

Table 3: Pressure Boundary, Sand and Air Flowrate

ASPECT RATIO	PRESSURE DROP (psi)	AIR FLOWRATE (lbm/s)	SAND FLOWRATE (lbm/s)
10	45	7.808e-3	2.98e-4
20	15	3.0e-3	1.68e-4
30	12	1.83e-3	2.34e-4
40	8	1.26e-3	2.9e-4

EXPERIMENT II

The setup for the second experiment was very similar to experiment one, except that all instrumentation was removed leaving only the pressure gauge at the mixing chamber connected. The pressure gauge at the nozzle was removed as it hinders the movement of the nozzle in the transverse and longitudinal axes during drilling operations.

Figure 4 shows the setup of the experiment, with the abrasive jet now impinges on to a two millimeter thick tool steel plate. The tool steel plate was mounted on to a fixture and held stationary. The nozzle was fixed in a holder which could translate in the X , Y and Z directions as depicted in the diagram. A simple computer program was written to move the nozzle across the tool steel and into position in the X and Y direction only. The movement in the Z direction was adjusted manually.

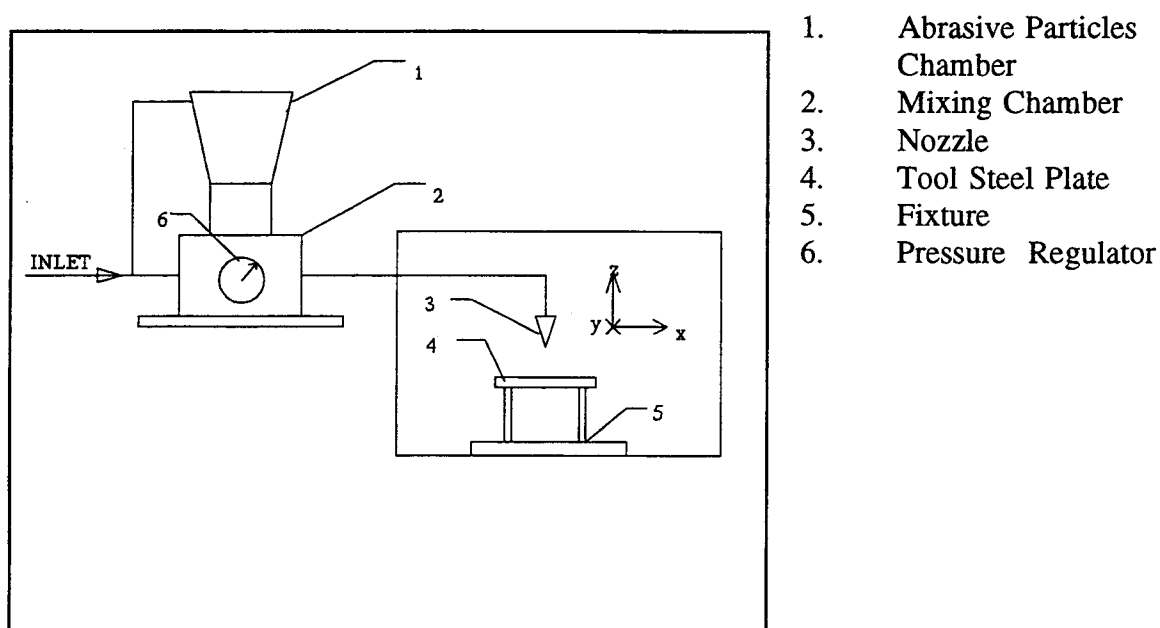


Figure 4: A Simplified Layout of Experiment II

A computer program was also written to instruct the nozzle to drill five times for a specified time interval. The time interval for each set of five drilling sequences ranged from five seconds to ninety seconds. At the end of the ninety second set, the standoff distance was adjusted to a new setting and the whole drilling process was

repeated. This experiment was conducted for the four nozzles and was performed at a nozzle inlet pressure of 80 psi.

With the same experimental setup, rectangular craters were created for the same range of standoff distances for all the nozzles. The drilling was performed with a dwelling time of 10 seconds at pressures of 30, 50, 70, 90, 110, 120, 130, and 140 psi respectively. Table 4 provides a listing of nozzle sizes for the experiment.

Table 4: Orifice Size of Nozzles

Aspect Ratio	Width (inch)	Length (inch)
10	0.0225	0.225
20	0.01125	0.225
30	0.0076	0.225
40	0.0056	0.225

A cross section of the nozzle is drawn in figure 5. The nozzles were connected to a constant size nozzle chamber. The length was the same for all the nozzles, the only dimension that was varying was the width of the nozzle orifice, see table 4.

Air carrying the particles flowed into the nozzle chamber and accelerated through the length of the nozzle. The abrasive jet was focused on the tool steel plate to drilled a rectangular slot. The size and depth of the craters were measured with laser metrology.

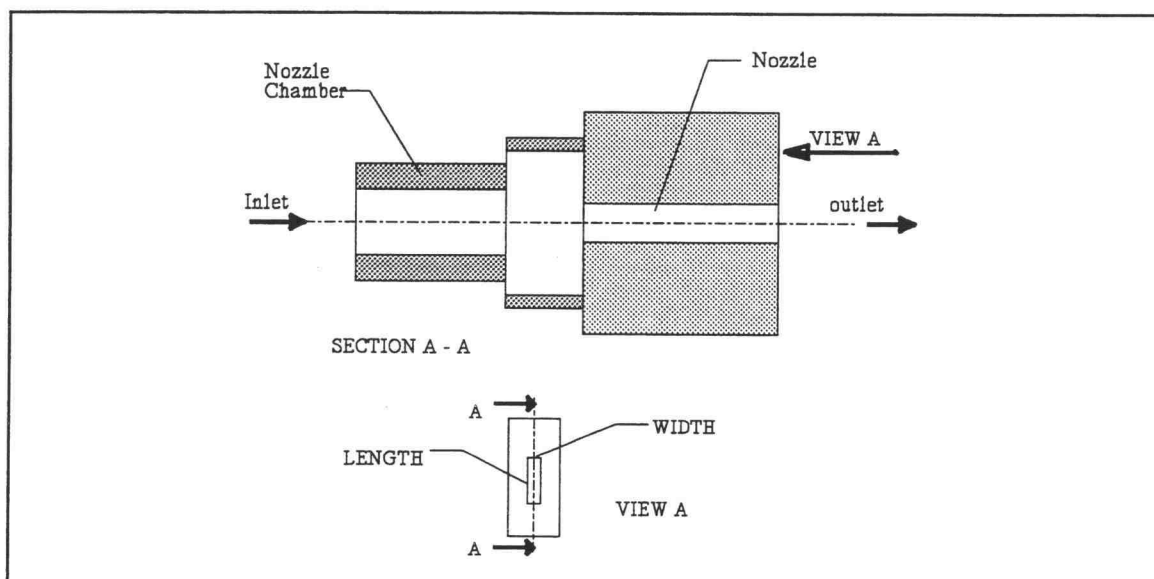


Figure 5: Nozzle Assembly

Experiment III

Various methods were considered for the verification of the results from computer modeling. A method such as Laser Doppler Velocimetry (LDV) was found to be the most appropriate, but was not available at this point in time. A force transducer was also considered as one of the methods to measure the impact force but because of the high abrasive nature of abrasive jet, this method of measurement was

also not suitable. Thus at this time in the project, it was decided that for verification of the computer modeling, only the air phase of the jet will be validated with the experimental results. This validation was done by measuring the stagnation pressure of the gas phase at the point of impact.

For verification of the two phase flow, the computer model "verification" was done by comparing the size and shape of the rectangular crater created by drilling to the abrasive particles distribution at the point of impact at the tool steel. Thus, the energy density profile of the solid phase jet could be represented by the impacted particle distribution at the plate, and the crater contour should be the energy " footprint " of the two phase jet. Computer verification of two phase jet was done only for aspect ratio 10 and 40 nozzles at NTS distance of 100 mils.

The experimental setup is shown in figure 6. The tool steel was replaced by a fixture with a pitot tube attached. The total pressure from the pitot tube was sensed by a SENSYM differential pressure sensor which had a maximum range of 150 psi. A Fluke 97 scopemeter was used to display and record the pressure.

As the output of the SENSYM differential pressure was in voltage, a calibration of the voltage to a USG pressure gauge was done. A linear relationship between the output voltage and pressure is shown in Figure 7.

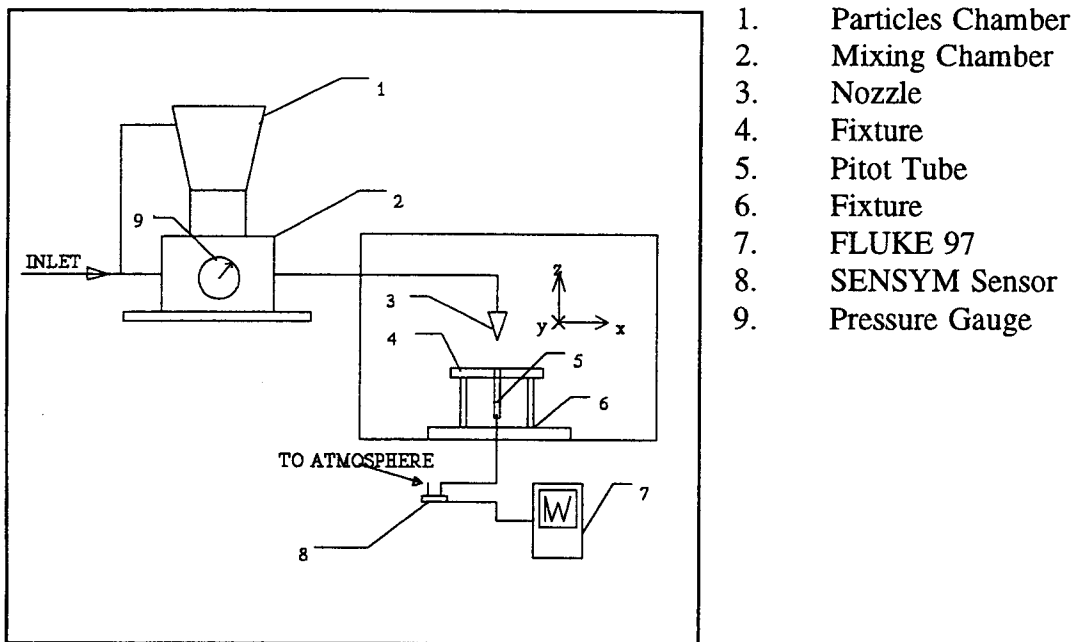


Figure 6: A Simplified Layout of Experiment III

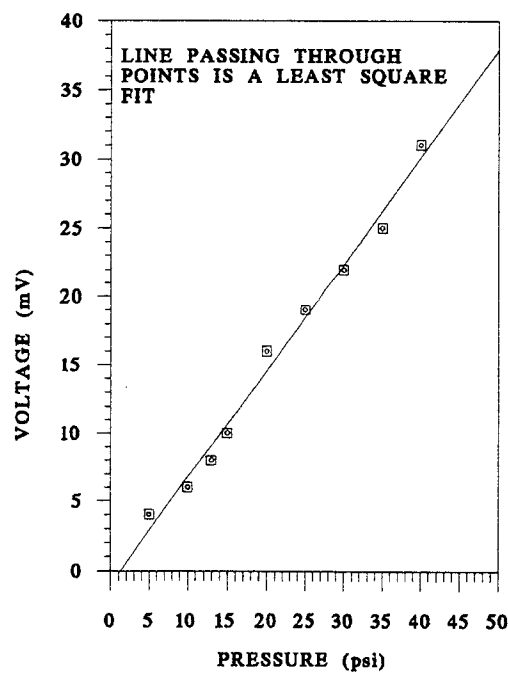


Figure 7: Pressure and Voltage Relationship SENSYM Sensor

NUMERICAL EXPERIMENT

The computer code that was used to model the rectangular abrasive jet was Fluent IV by Fluent Inc, Lebanon, New Hampshire. Fluent is a general purpose computer fluid dynamic code capable of modeling a large variety of fluid flow phenomena. In Fluent, the user inputs model assumptions that best represent the physical situation. Fluent uses a control volume based technique to convert the most general cases of differential conservation equations to algebraic equations which can be solved numerically. This control volume technique consists of integrating the differential equations about each control volume. This yields a finite difference equation that conserves each quantity on the control volumes basis.

Fluent, besides solving the transport equations for a single continuous phase, can also solve a dispersed second phase. The code assumes that the second phase consists of spherical particles dispersed in the continuous phase. In addition to that, the second phase is also assumed to be sufficiently diluted and the effects of the particle volume fraction on the gas phase are negligible. Fluent uses a Lagrangian formulation to calculate the trajectory of the particles by equating the force balance of the inertia force and the force acting on the particles.

For the numerical representation of the experiment on rectangular nozzles, a set of input parameters and boundary conditions were obtained through experiment for all the nozzles. The physical properties of the carrier fluid and the particles are shown in table 5.

Table 5: Materials Properties

Property	Gas	Particle	Units
Density	Func of Pressure	243.7	lbm/ft ³
Thermal Conductivity	1.46e-2	6.35	BTU/hr ft R
Specific Heat	2.398	0.1911	BTU/lbm R
Viscosity	1.21e-5	not needed	lbm/ft-sec

Because of the symmetry involved in the problem, only half of the entire nozzle needed to be modeled. Several assumptions were made to simplify the computation as much as possible but, at the same time, modeled as close to the actual experimental model. The flow of model was assumed to be at steady state. The nozzle was modeled with no heat flowing across the wall with a jet discharging into ambient pressure which was at atmospheric. Also the flow was assumed to be turbulent and compressible and gravitational force was neglected.

For the flow of the second phase, it was assumed that no heat transfer takes place between the particles and the plate during impact and the particles do not disintegrate after impact with the plate.

The inlet and exit velocity was calculated first based on the inlet pressure of 80

psi. It was found that the velocity was subsonic at the inlet and supersonic at the outlet. But in the numerical model, the flow was assumed to be discharging into a plenum, see Figure 9. The eventual exit velocity (at the edge of the plenum) will be subsonic. Therefore, the nozzle was modeled having a transonic flow with subsonic inflow and subsonic outflow but was supersonic in between the two.

The numerical experimentation was divided into two parts. In the first, a converged steady state solution was obtained for the pure gas jet. This single phase flow solution was then used as a flow field for performing the particle calculation. A total number of eleven injection points were used to simulate the flow of the particles. These injection points were located at the inlet of the nozzle chamber, as shown in Figure 8.

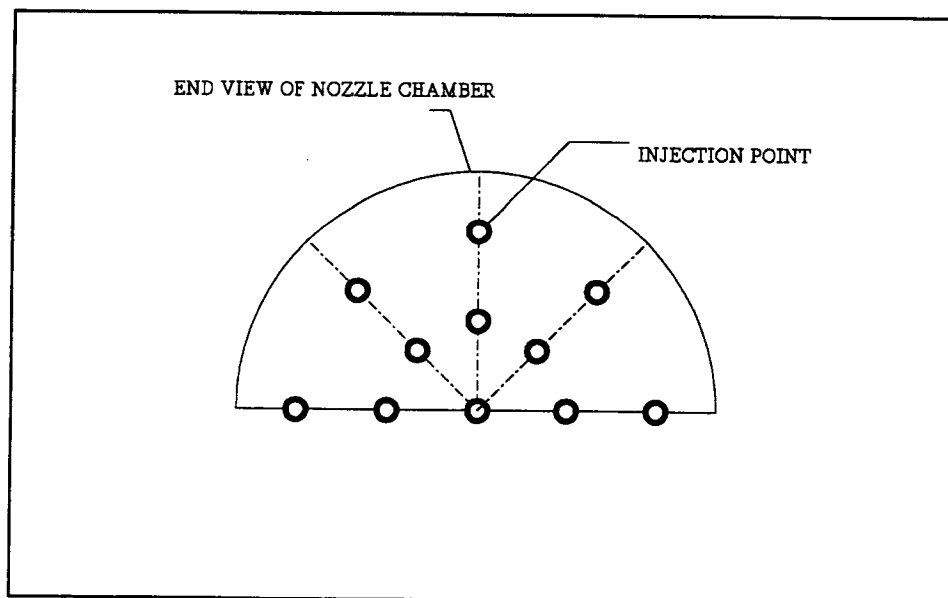


Figure 8: Position of Injection Points for Modeling

Each injection point will have five bins and the particle size distribution at the injection points was represented by the Rosin - Rammler expression. The mass loading for each nozzle was found in experiment I, see table 3

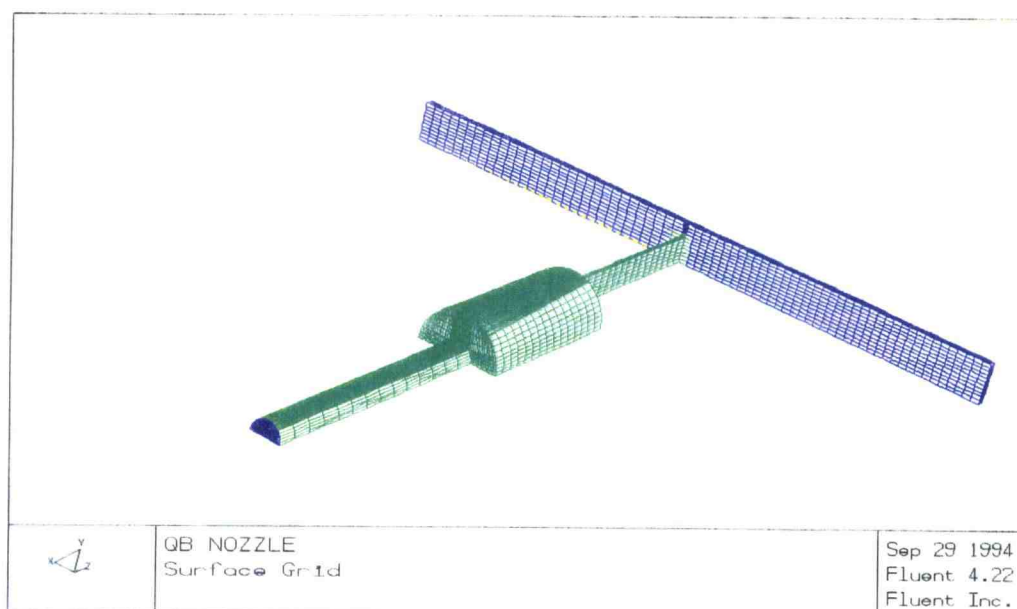


Figure 9: Geometrical Meshing of Nozzle

An outline of the computational geometry representing a nozzle and a plate is shown in Figure 9. The outline showed the internal flow area of the nozzle discharged into a plenum. The face of the plenum facing the nozzle exit is closed, thus

representing the plate. The other sides of the plenum are opened to provide for entrainment effect or exit of the jet. The meshing of the nozzle shown in Figure 9 has flow area represented by green, plane of symmetry by yellow and inlet and outlet by blue. Selected slices of the computational domain are shown in Figure 10. The size of the computer domain is $80 \times 15 \times 80$ nodes.

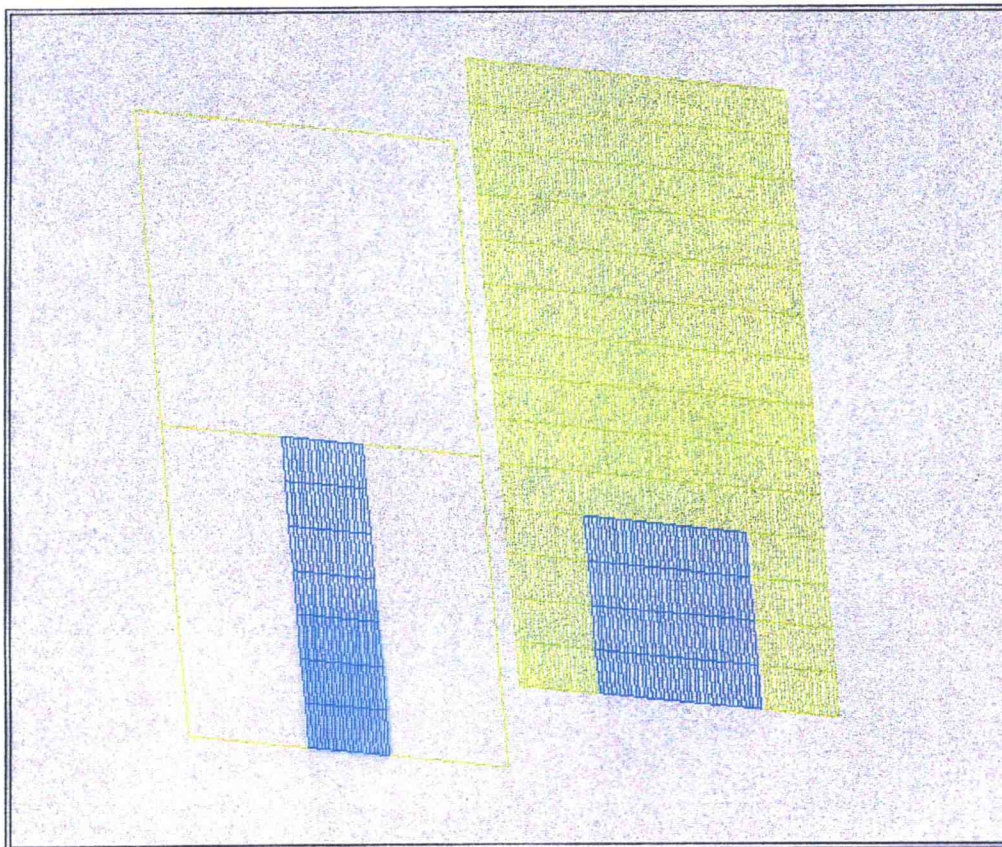


Figure 10: Selected Slices of Model in Computational Domain

RESULTS

In this section, the results from Experiment II are used to discuss the trends of the experimental data. This is done in hopes that nozzle designers can use these trends to anticipate the size of the hole drilled from the nozzle orifice on which the designer has decided on. Experiment I and III will be combined to evaluate the suitability of a numerical code for nozzle design applications.

EXPERIMENT I

Measurement of the air flowrate and abrasive flowrate reveal that the air flowrate increases with nozzle size but the abrasive flowrate does not. Figure 11 shows that nozzles with aspect ratio of 10 and 40 have almost the same sand flowrate but aspect ratio nozzles 30 and 20 have a smaller flowrate see (Figure 11). The reason behind these unexpected results can best be explained by plotting the abrasive flowrate against a range of nozzle inlet pressure. The curves in Figure 12 show that for an inlet pressure of 80 psi, the flowrates of aspect ratio 10 and 40 nozzles are at optimum. But for aspect ratio 30 and 20 nozzle, both of the nozzles have a peak flowrate at 100 and 120 respectively. Thus with these two graphs it can be deduced that even though the air flowrate is dependent on the area of the nozzle, the abrasive flowrate is a function of both the nozzle area and the nozzle inlet pressure.

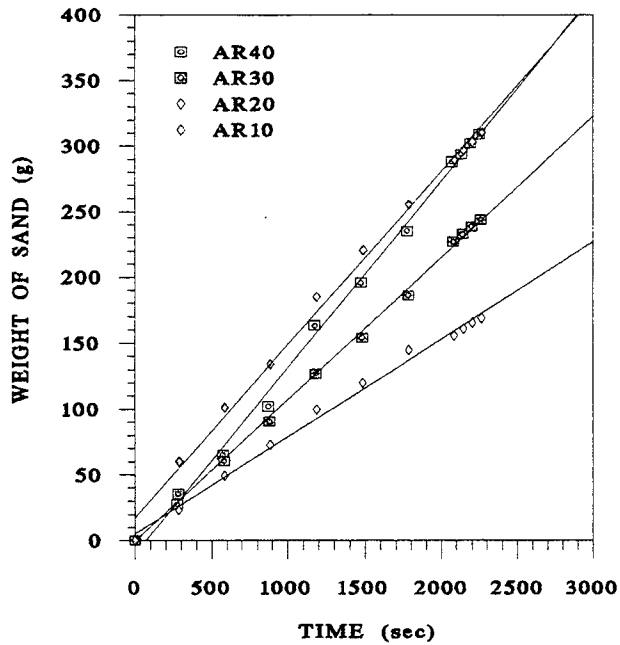


Figure 11: Sand Flowrate for All Nozzles at Inlet Pressure of 80 psi

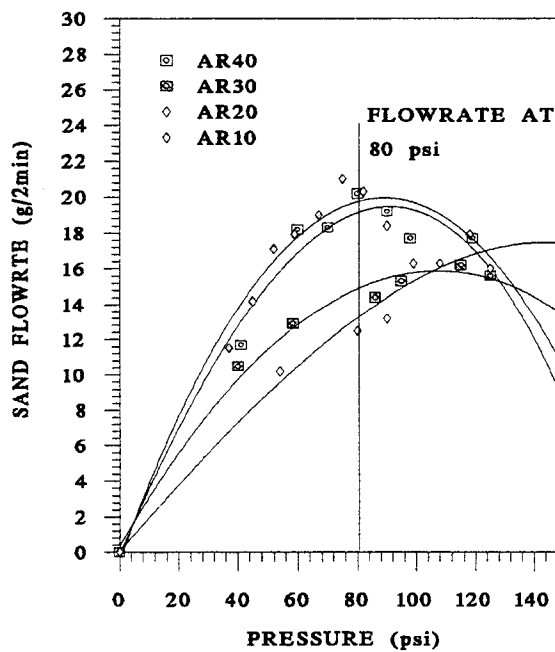


Figure 12 : Sand Flowrate with Respect to Nozzle Inlet Pressure

The results also show that the particles mass flowrate is diluted when compared with the air mass flowrate of each respective nozzle. A nozzle with an aspect ratio of 10 has a abrasive flowrate of only 4% of the air flowrate, whereas a nozzle with an aspect ratio 20 has 5.6% , aspect ratio 30 nozzle has 12.7% and aspect ratio 40 nozzle has 23.3% of the air flowrate.

EXPERIMENT II

TIME EFFECT

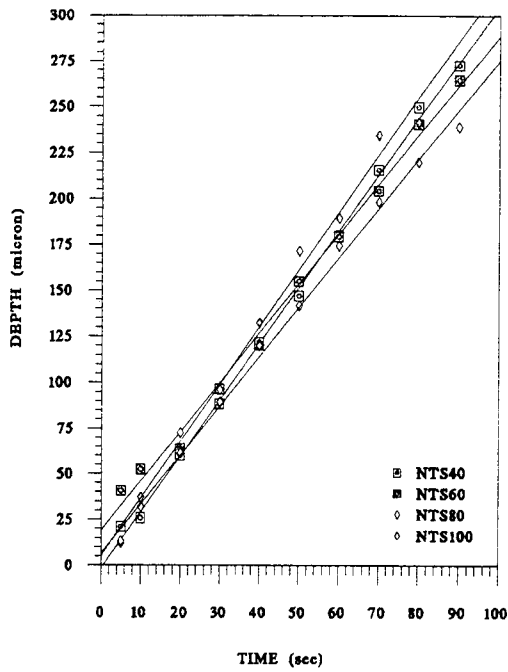
In Figures 13a to 13d a least square fit was used to show the effect of time on the penetration depth of the nozzles at various nozzle to substrate (NTS) distances. The graphs show that the increase in depth is approximately linear after the initial starting transient. In Figures 14a to 14d the plots show the length of the rectangular craters throughout the drilling duration at all the standoff distances shows only a slight increase in length . The length stays almost constant at about 6000 micrometers which is an increase of only 4.98 % of the nozzle orifice length . The effect of time on the change in width is shown in Figures 15a to 15d. It is observed that the width follows an increasing linear trend for all aspect ratio. The size of the width also increases as the NTS distance is increased, except for aspect ratio 40 nozzle where the width of the rectangular crater at an NTS distance of 100 mils are smaller than those at other NTS distances.

The behavior of the trends shown above can be explained if one looks at the

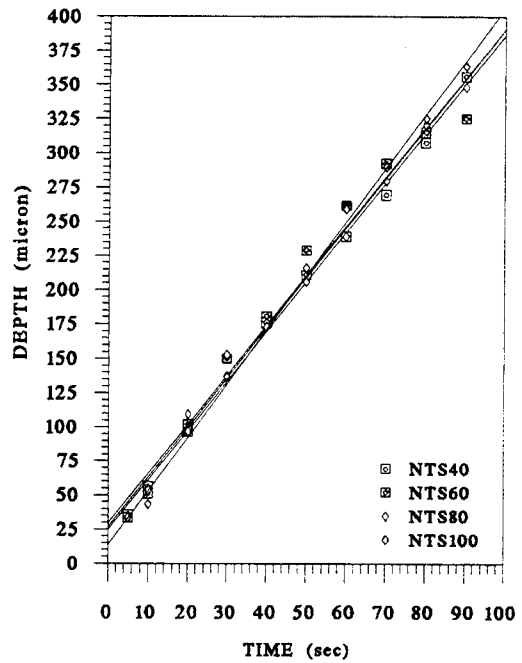
structure of a two phase jet, as shown in see figure 16. As can be seen from the diagram, a particle jet exists inside the gas phase jet (Sommerfeld, 87); Erosion of the plate is caused by the particle jet force introduced to the surface of the plate.

The particle jet gets its energy from the velocity it gained from the carrier gas.

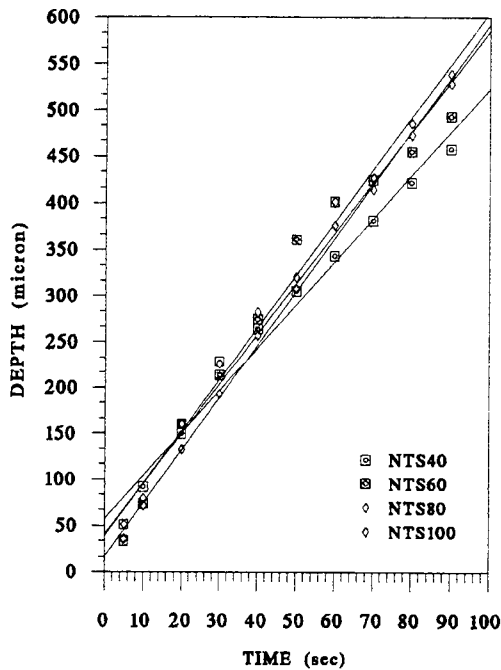
The energy supplied by the particle jet to the plate is given by the product of the particle jet force and the loading time. Since momentum and the jet force are related, the energy distribution of the particle jet can be assumed to be similar to the contour of the crater. That is the shape of the crater can be assumed to be the imprint of the two phase jet energy.



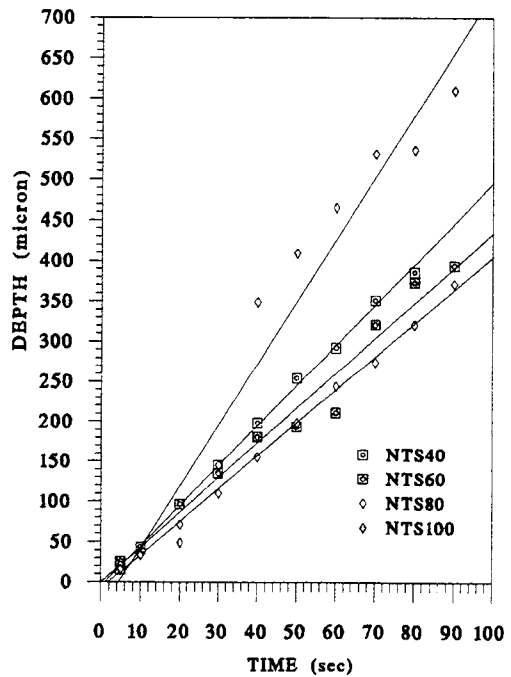
(a) Aspect Ratio 10



(b) Aspect Ratio 20

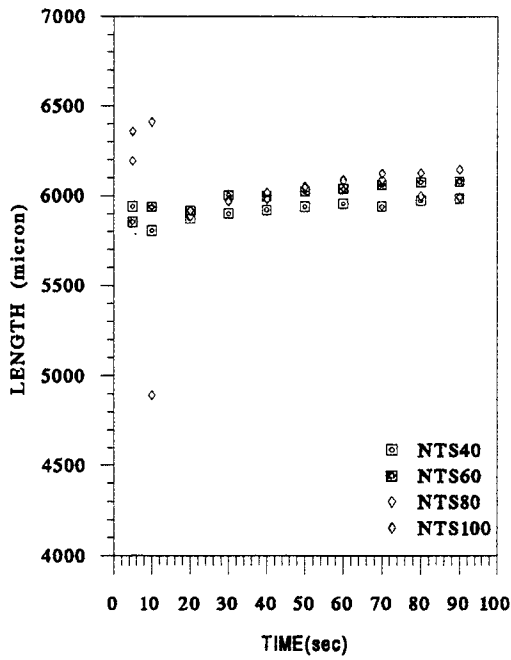


(c) Aspect Ratio 30

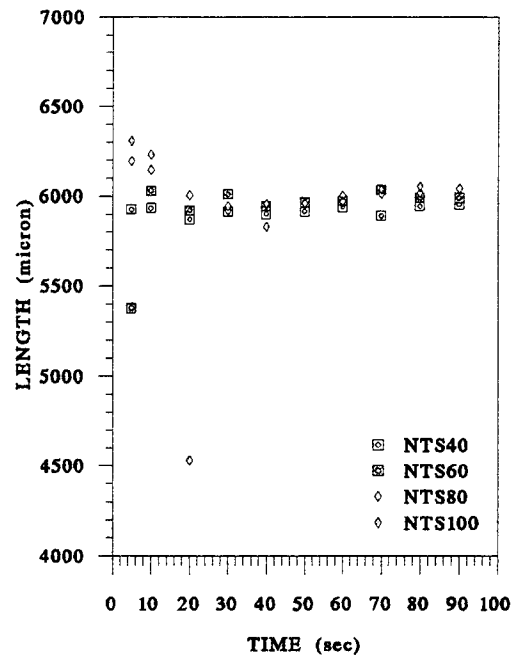


(d) Aspect Ratio 40

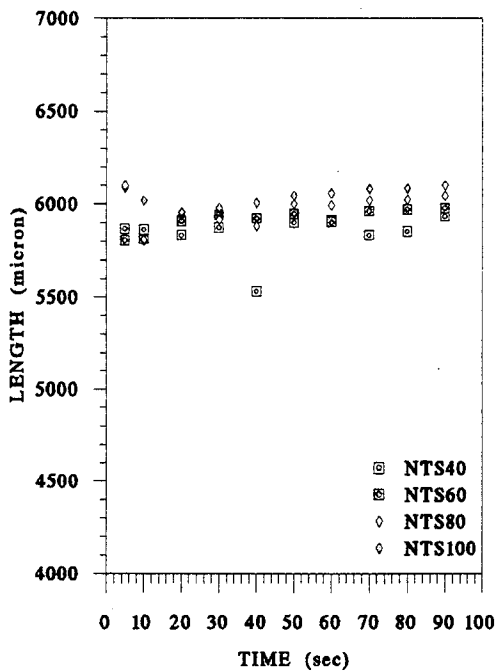
Figure 13a to 13d: A least Square Fit of the Time Effect on Penetration Depth for All Nozzles and at All NTS Distances at an Inlet Pressure of 80 psi



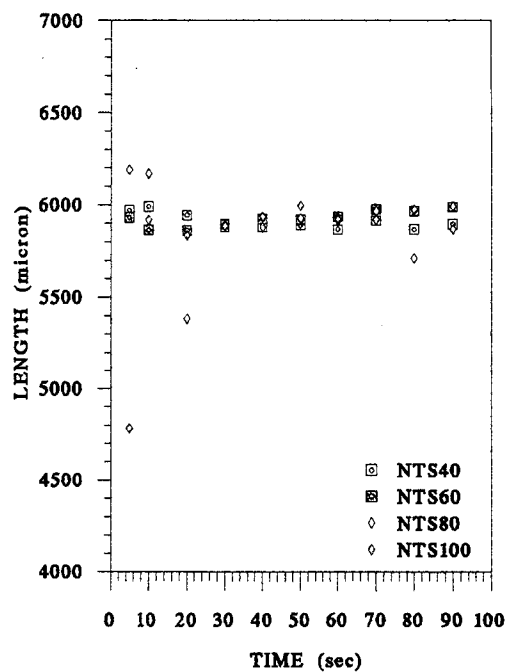
(a) Aspect Ratio 10



(b) Aspect Ratio 20

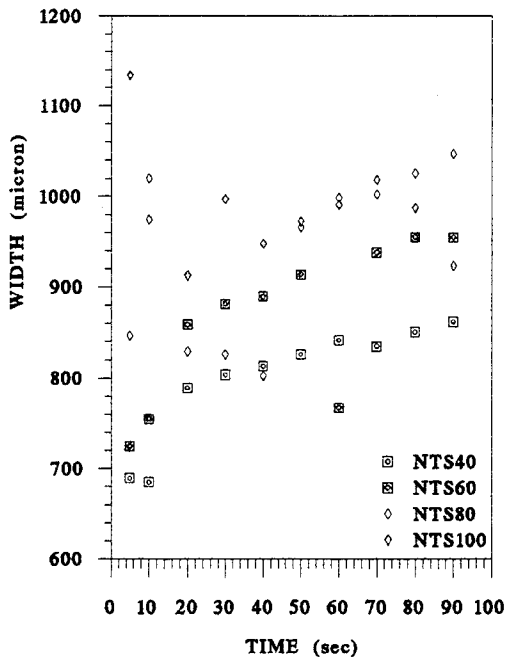


(c) Aspect Ratio 30

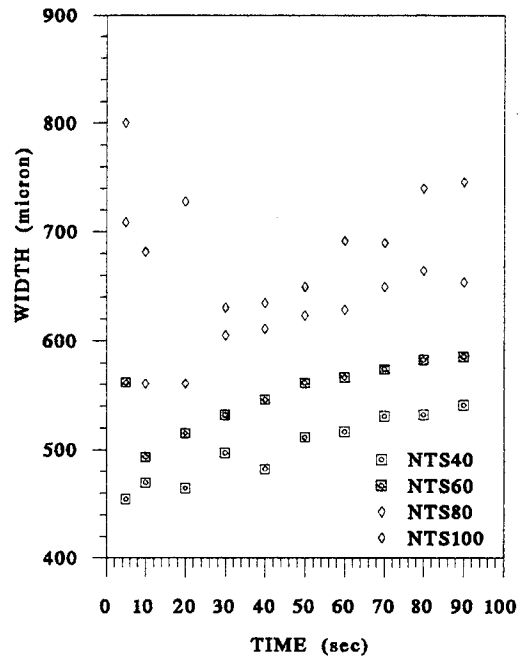


(d) Aspect Ratio 40

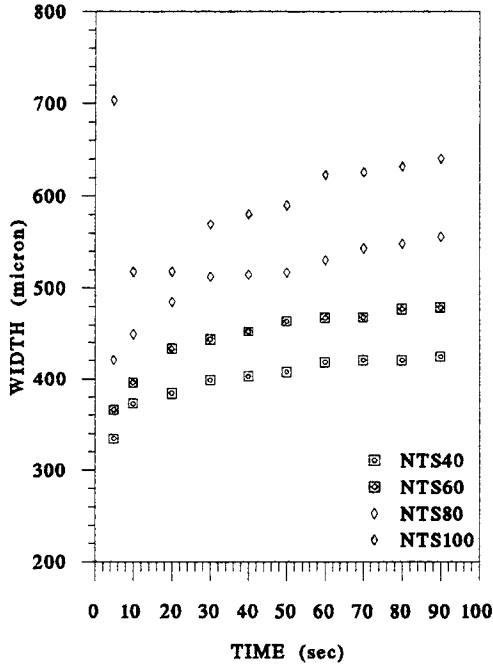
Figure 14a to 14d: Time Effect on Length for All Nozzles and at All NTS Distances at an Inlet Pressure of 80 psi



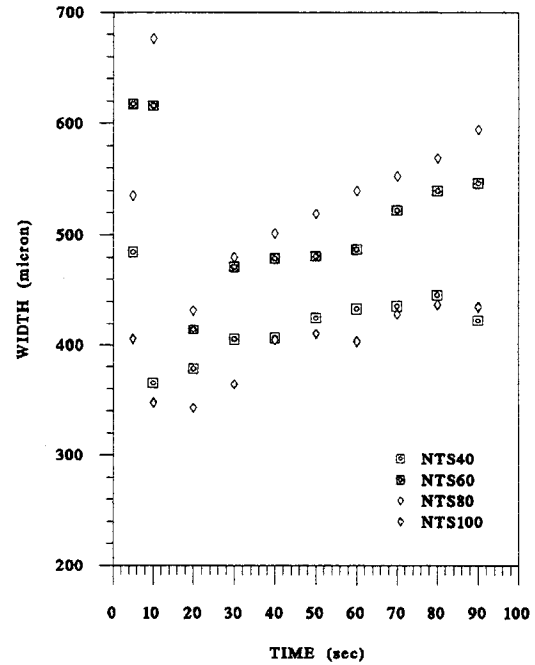
(a) Aspect Ratio 10



(b) Aspect Ratio 20



(c) Aspect Ratio 20



(d) Aspect Ratio 40

Figure 15a to 15d: Time Effect on Width for All Nozzles and at All NTS Distances at an Inlet Pressure of 80 psi

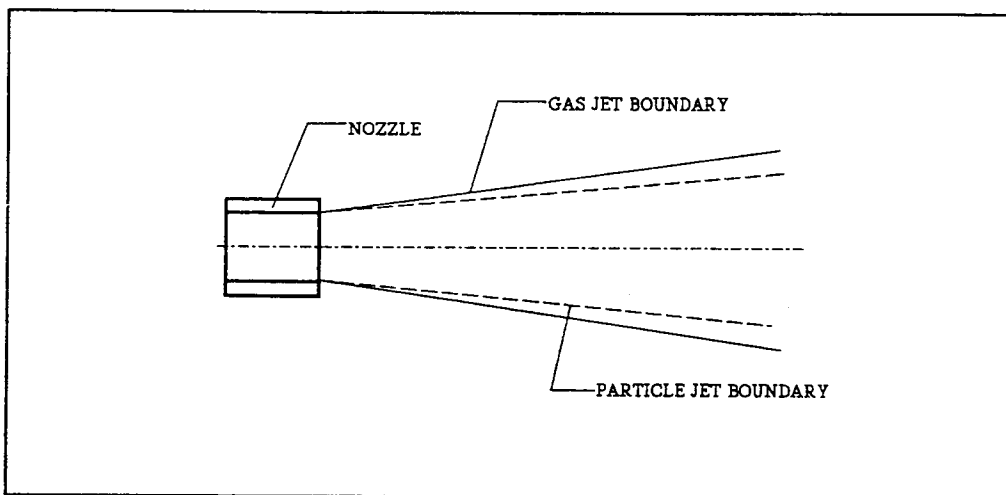


Figure 16: Structure of Two Phase Jet

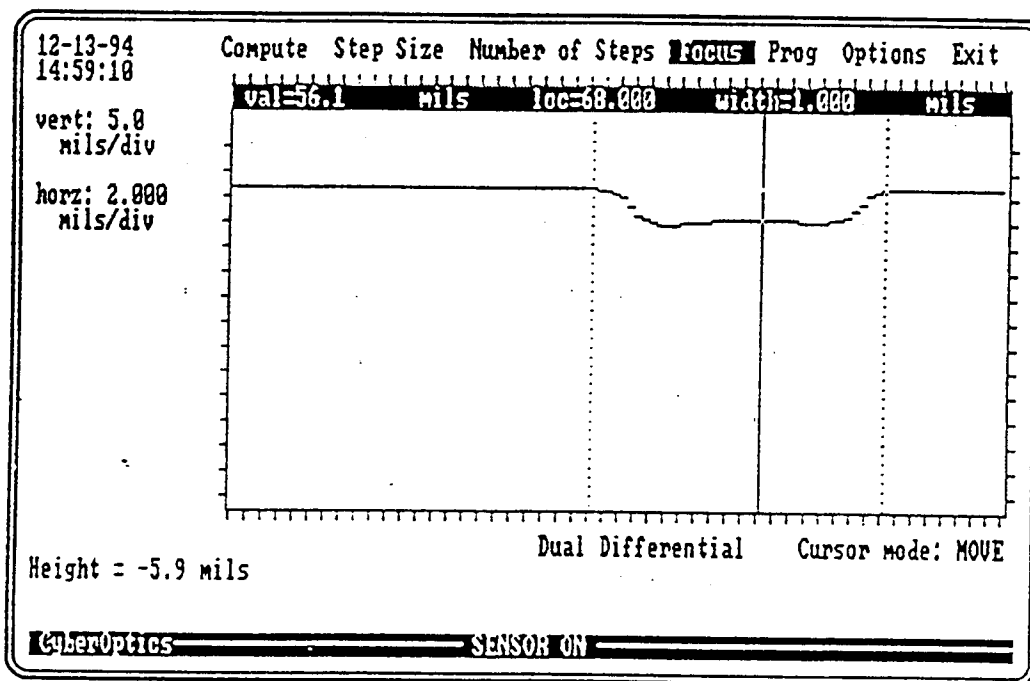


Figure 17a: Laser Scan of Crater Across the Length

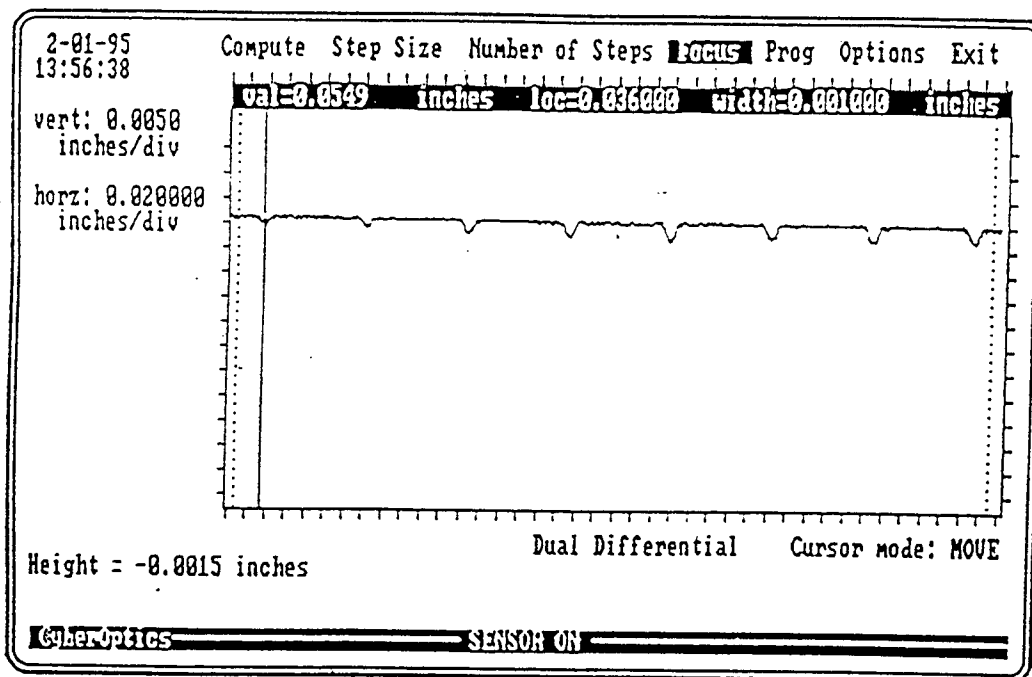


Figure 17b: Laser Scan of Multiple Craters Across the Width

Using laser metrology, a scan of the crater contour is made, (see Figure 17a and 17b) . The figures show that the crater has an inverted saddle shape with straight sides along its length whereas the scan across the width shows a sharp needle like profile.

The widening of the slots can be best explained by the work of W. Konig and Ch. Wulf (1984) on round nozzles. W. Konig and Ch. Wulf theorized that the dependency of the slots geometry on the influencing parameters, the structure of the jet has to be taken into account. They theorized that the gaussian distribution velocity profile of the jet will be transferred to the surface of the plate.

By borrowing their theory and used the contour in the slot to represent the velocity profile of the jet. The dependency of the slot width becomes evident. When the loading time is increased, which is equivalent to a reduction power of demand for penetration. The power requirement changes from D1 to D2 as shown in the energy sketch in figure 18. Thus the active size of the jet and hence the length of cut grows from L1 to L2. Because of the almost straight edges, the change of the length is minimal; L1 to L2 .

Looking across the width the same explanation can be provided; with longer dwelling time the demand for energy is lowered as above, thus the power requirement changes from P1 to P2, hence the growth of the width drilled changes from W1 to W2. The same explanation is given for the growth of the width as NTS distance increases. At a larger NTS distance, the energy distribution is flatter, shorter, and weaker, and hence a wider width at larger NTS. However if the NTS distance is too far the energy profile that can actually produce the drilling will be too weak. Thus in this case only the tip of the energy profile has sufficient energy to penetrate the plate. This accounts for the smaller crater width for aspect ratio 40 nozzle at NTS of 100 mils.

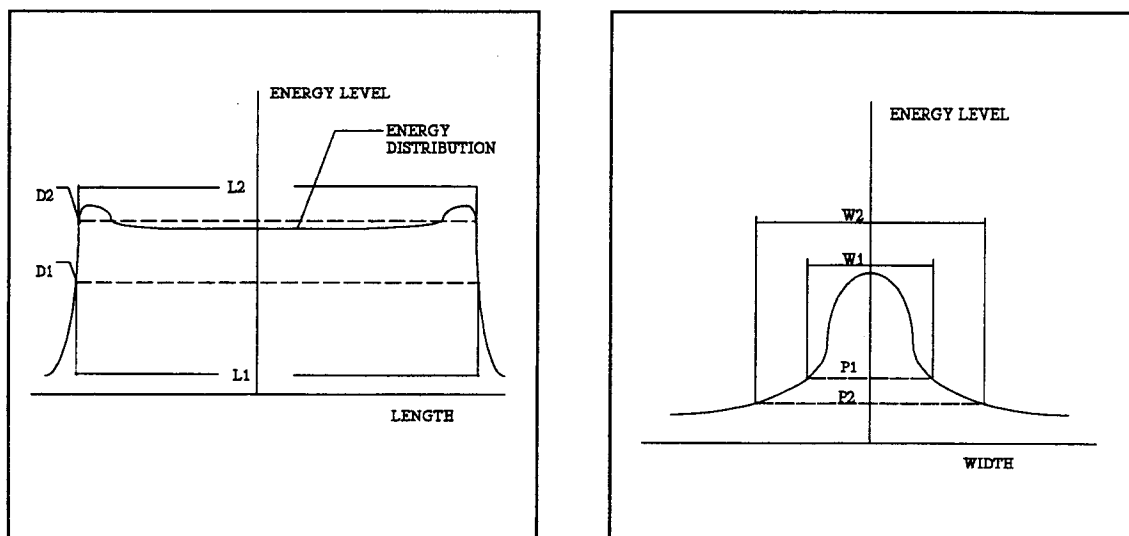


Figure 18: Energy Distribution and Resulting Width and Length

EFFECT OF AIR PRESSURE

Experimental observations of the effect of pressure on the penetration rate is shown in Figure 19a to Figure 19d. The graphs show that the penetration rate increases with increase in nozzle pressure. This rate of increase of penetration decreases with increasing nozzle pressure and has the tendency to level off at some value of pressure. Depending on the operating NTS distance, the optimum operating pressure where the penetration depth is the greatest, occurs for the geometries used between 100 and 120 psi. By extrapolating each trend backward, each penetration curve intersects the pressure axis at a particular critical pressure P_c .

The change of length of the craters in Figure 20a to Figure 20d, like the effect of time, appears to remain constant at 6000 micrometers for all the nozzles and at all

the NTS distances. The pressure effect on the width however projects an increasing trend in Figure 21a to Figure 21b. However, the rate of change of the width has the tendency to saturate at some value of nozzle pressure at higher NTS distances.

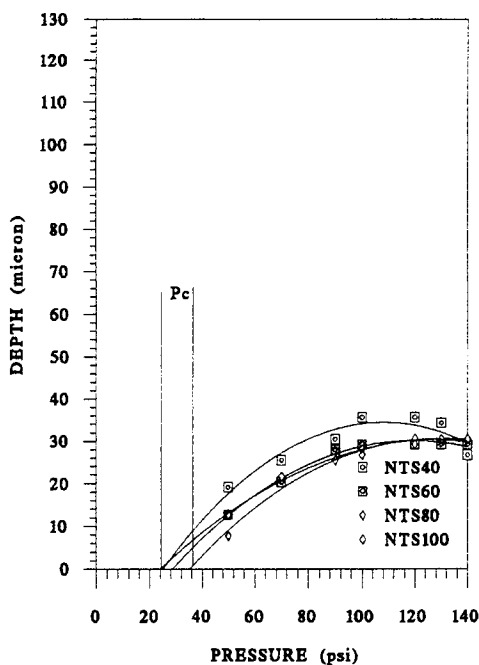
The growth of the width and length in this case is again due to the energy distribution of the particle jet. At higher pressure, and at a fixed dwelling time, the jet will penetrate deeper into the material. From the energy curve in Figure 18, the power requirement level on the surface of the plate is at P2 and hence the active jet width. The limited growth of the length is again due to the straight sides of the energy contour.

The leveling off of the penetration depth is because of the inertial effect of the suspended particles and also because the operating pressure and the mass loading have to compromise each other. When the carrier gas leaves the nozzle exit, it attains a maximum velocity outside the nozzle exit before it starts to slow down. The abrasive particles, being heavier, lag behind and continue to accelerate. At some point in the jet region the slip velocity between the abrasive particle and the gas will be zero; i.e. the carrier gas and the abrasive particles are at the same velocity. Beyond this point the jet flares out significantly and the abrasive particle velocity decreases to a point where no erosion can occur.

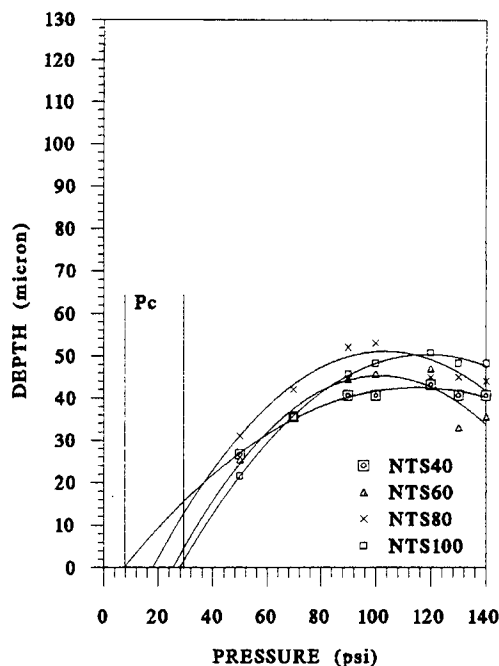
Finnie (1960) has shown that the erosion rate is a function of the impacting particles velocity and mass flowrate. The leveling off of the penetration curve is due to the maximum velocity attained by the particles before collision at that particular NTS distance. The maximum velocity of the particles also depend on the mass

loading of the particles (Vermal and LAL, 85). With a smaller mass loading at a given operating pressure, less particles will be exposed to acceleration by the gas, thus a condition of small particle drag exists, hence a small operating pressure is required. In this experiment, the mass loading is controlled by the fluctuations of the shuttle valve therefore an accurate control of the mass flowrate of the abrasive particles is impossible. Because the inability to control the particle flowrate, the mass loading was assumed to be fixed. With a fixed mass loading assumed, the experiment was carried out by varying the operating pressure. The saturation of the penetration depth signifies that maximum momentum imparted to the particles has reached its limit and therefore further penetration is not possible. At this depth a balance is reached between the mixing ratio of the particles and gas with the operating pressure.

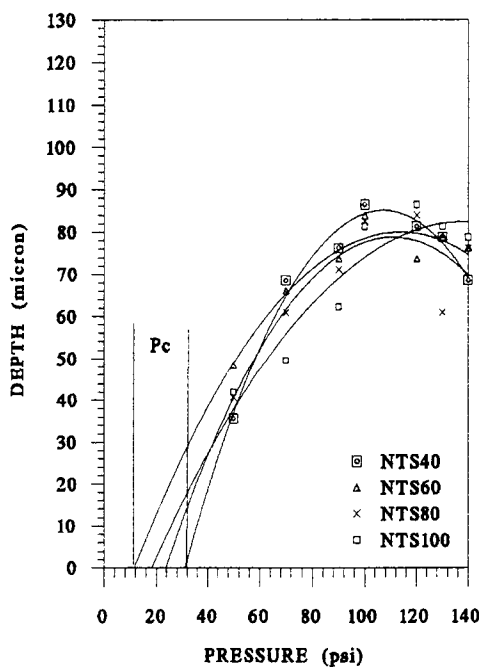
The critical pressure, P_c , is related to the critical particle velocity, which is also the material erosion characteristic as explained above. As mentioned before, the particles escape from the nozzle at a velocity lagging behind the gas velocity and will continue to accelerate. The erosion of the plate is due to the energy transferred from the particles which then must attain a minimum velocity before erosion can occur. Therefore, for a fixed mass loading, an operating pressure might not be high enough for the particles to acquire a minimum impact velocity in order to achieve erosion. The critical pressure, P_c then is the minimum operating pressure where the particles were able to attain minimum velocity for erosion to occur. At this pressure, it signifies that a balance between the mass loading and the critical pressure for minimum erosion to take place is reached.



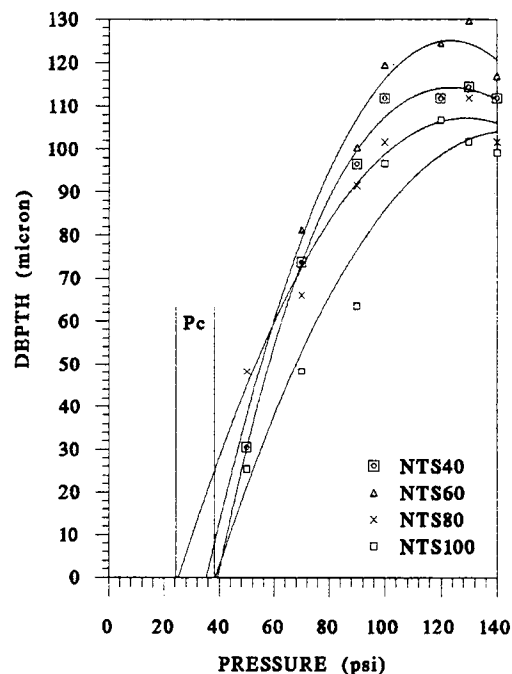
(a) Aspect Ratio 10



(b) Aspect Ratio 20

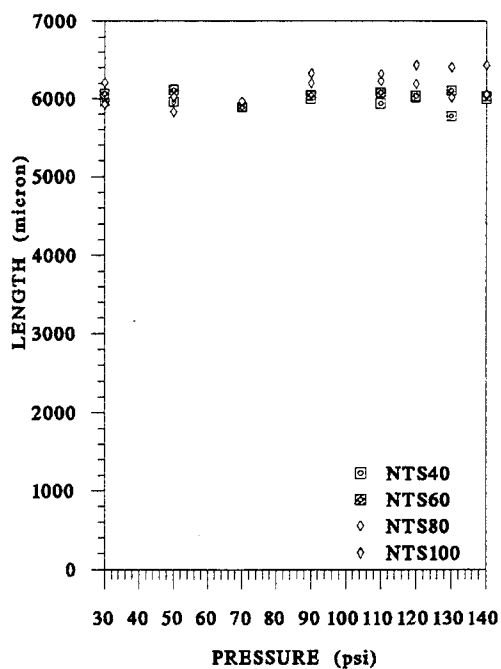


(c) Aspect Ratio 30

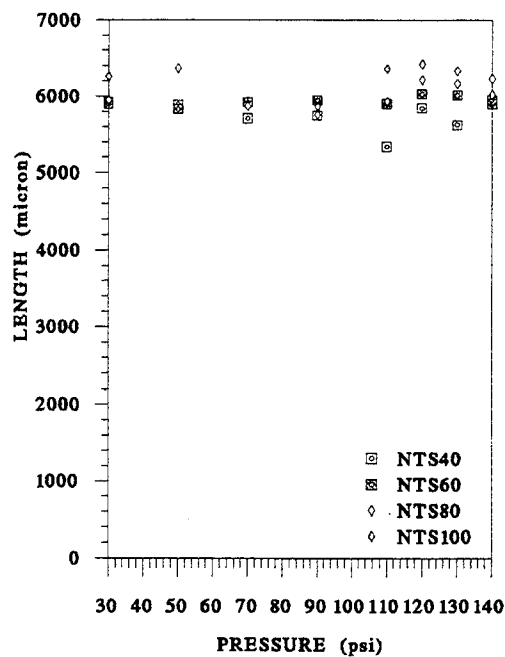


(d) Aspect Ratio 40

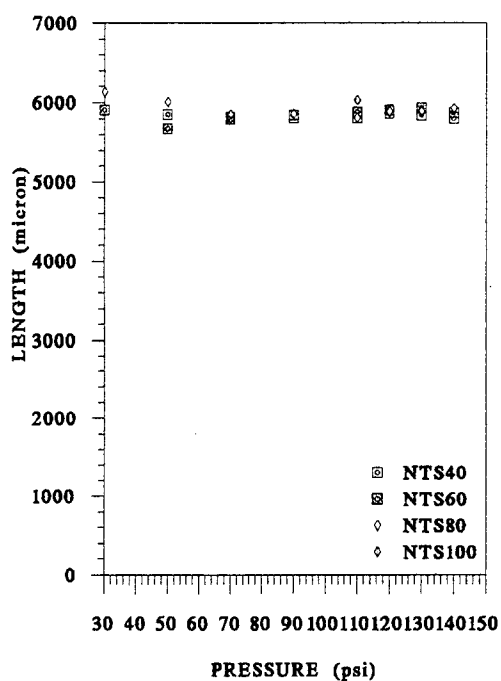
Figure 19a to 19d: 2nd Order Polynomial Fit of Pressure Effect on Penetration Depth for All Nozzles and at All NTS Distances with Dwelling Time of 10 Seconds



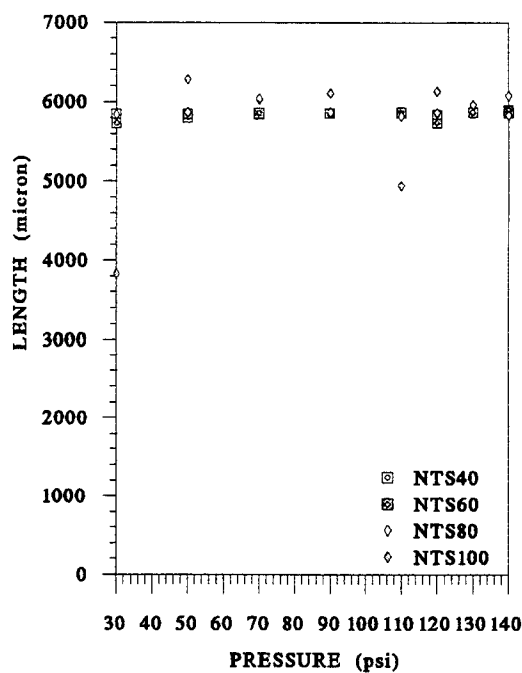
(a) Aspect Ratio 10



(b) Aspect Ratio 20

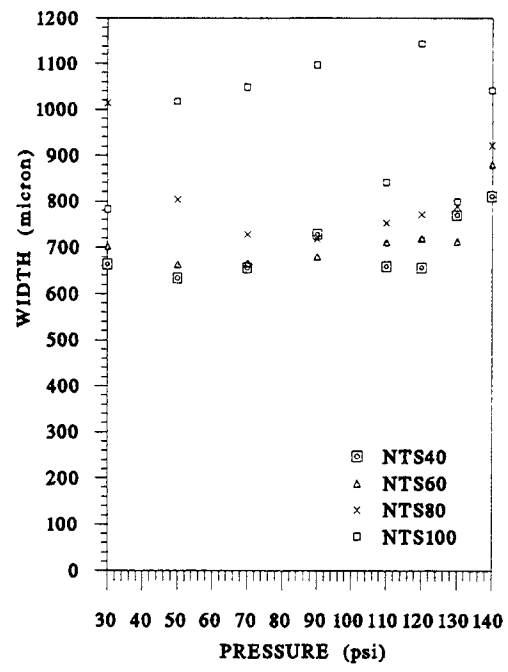


(c) Aspect Ratio 30

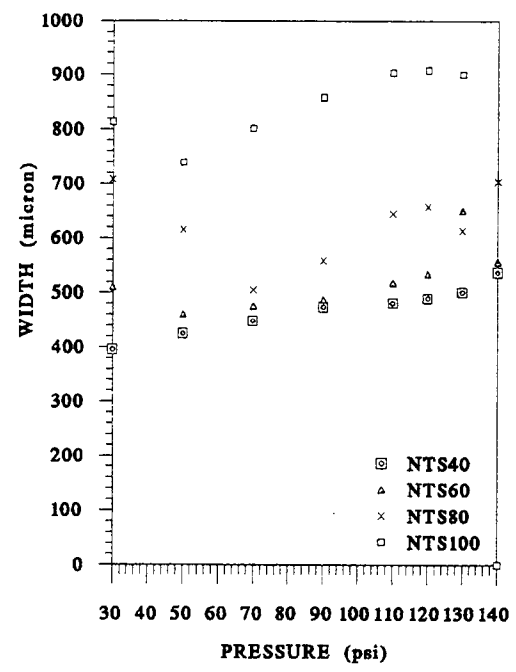


(d) Aspect Ratio 40

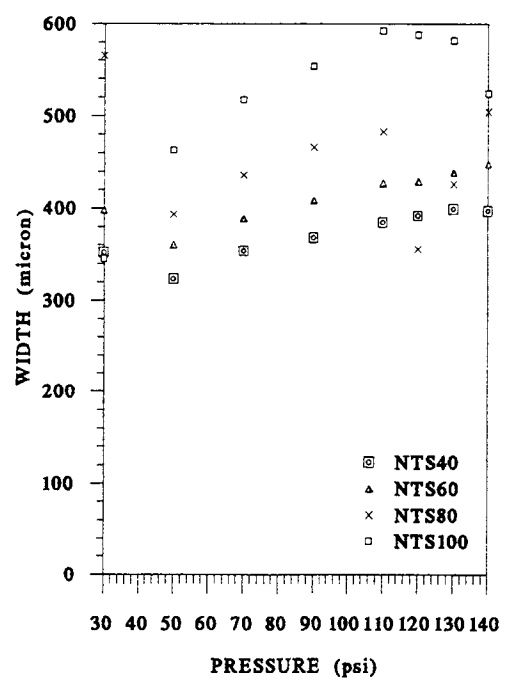
Figure 20a to 20d: Pressure Effect on Length for all Nozzles and at All NTS Distances with Dwelling Time of 10 Seconds



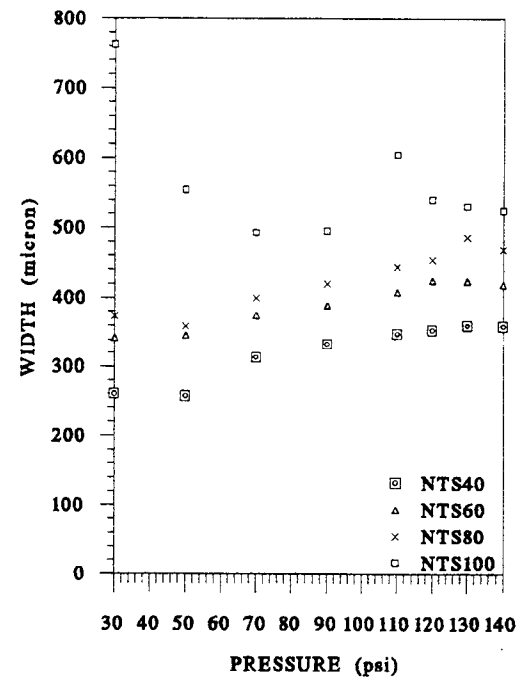
(a) Aspect Ratio 10



(b) Aspect Ratio 20



(c) Aspect Ratio 30



(d) Aspect Ratio 40

Figure 21a to 21b: Pressure Effect on Width for All Nozzles and at All NTS Distances with Dwelling Time of 10 Seconds

EXPERIMENT III

EVALUATION OF NUMERICAL METHOD

To evaluate the applicability of FLUENT for nozzle design, a gas phase flow simulation was performed first, and the results of the converged solution were compared with those collected from experiments. As for the two phase flow jet, because of the unavailability of suitable measuring instruments at this point in time to measure the two phase jet. The validation of the two phase flow results from FLUENT will be used strictly by comparing the physical interactions of the abrasive particles with the tool steel plate and the nozzle.

Plots of the velocity contours of the converged solution of the gas phase flow for all nozzles at all NTS distances are shown from Figure 22 to Figure 37. Figure 38 to Figure 41 shows the plots of the velocity contours of the nozzles at an NTS distance of 100 mils with particles injected. From the plots it can be seen that jets from aspect ratio 10 and 20 nozzles are in the potential core and thus the jets are stronger than those from aspect ratio 30 and 40 nozzles. In addition, the particles in the jet stream do not seem to have much effect on the jets width except to reduce the jets velocity.

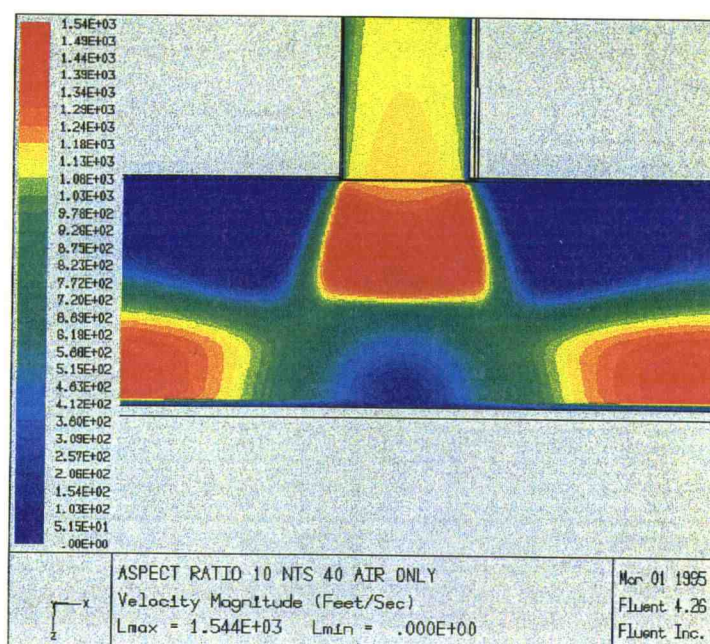


Figure 22: Velocity Contours of Single Phase Gas Jet for Aspect Ratio 10 Nozzle at NTS 40

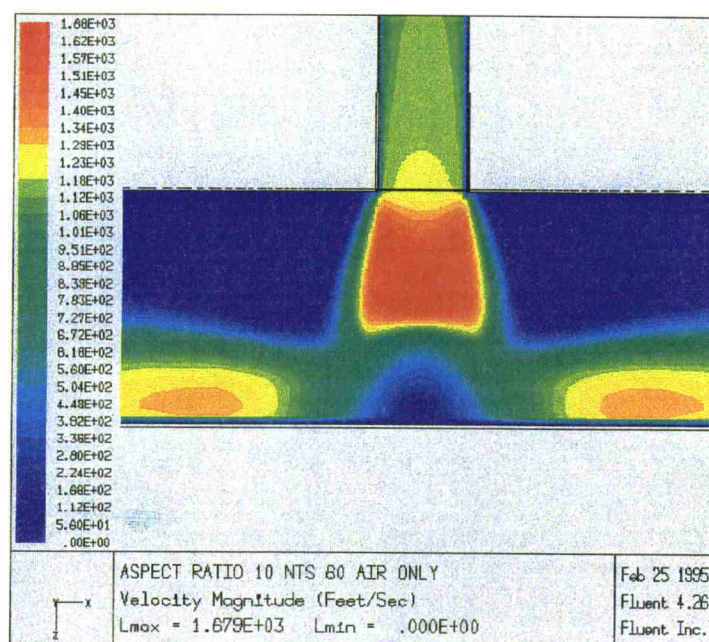


Figure 23: Velocity Contours of Single Phase Gas Jet for Aspect Ratio 10 Nozzle at NTS 60

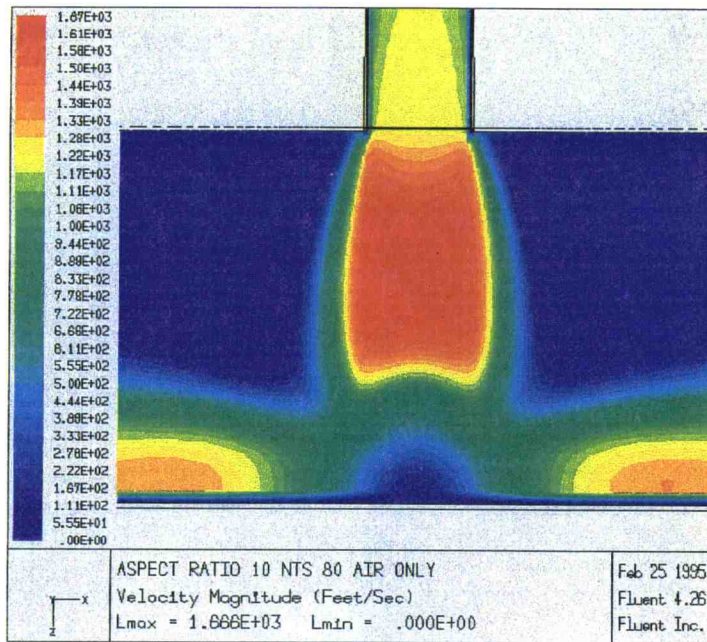


Figure 24: Velocity Contours of Single Phase Gas Jet for Aspect Ratio 10 Nozzle at NTS 80

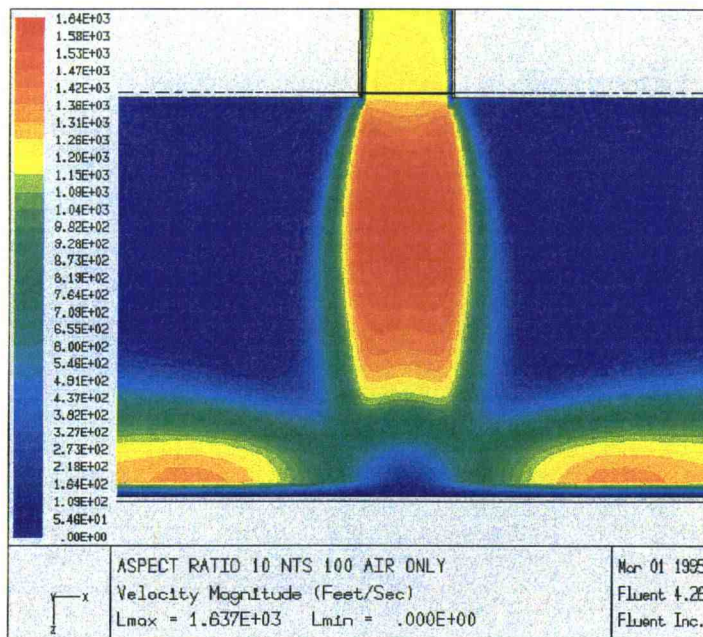


Figure 25: Velocity Contours of Single Phase Gas Jet for Aspect Ratio 10 Nozzle at NTS 100

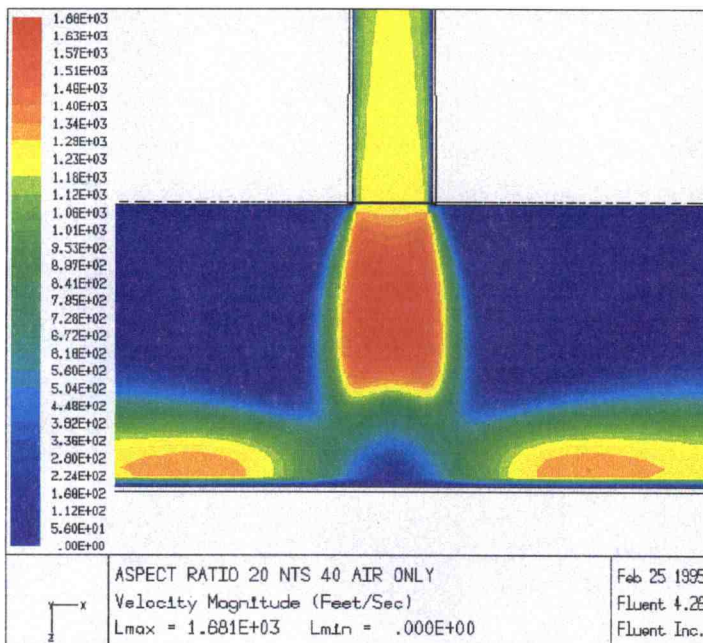


Figure 26: Velocity Contours of Single Phase Gas Jet for Aspect Ratio 20 Nozzle at NTS 40

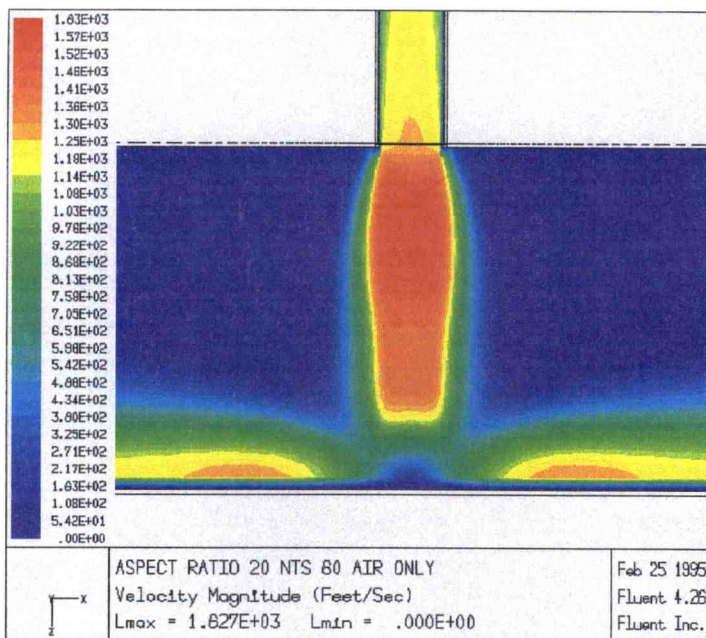


Figure 27: Velocity Contours of Single Phase Gas Jet for Aspect Ratio 20 Nozzle at NTS 60

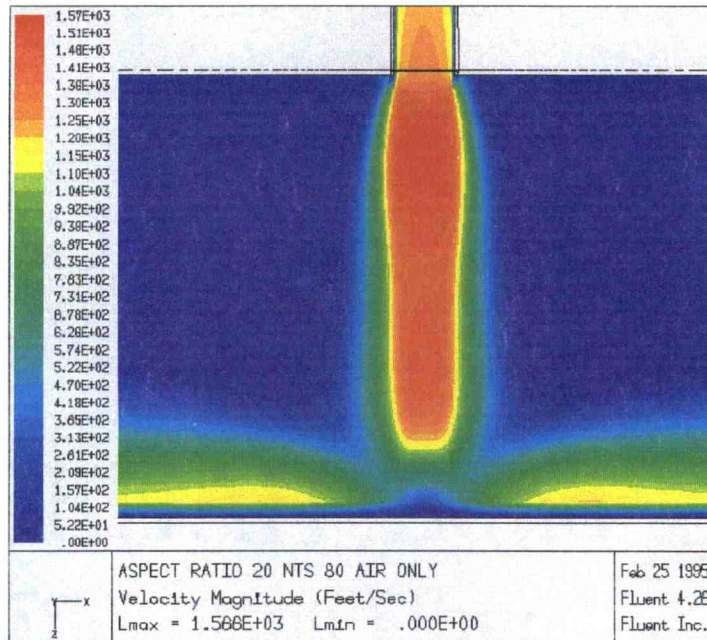


Figure 28: Velocity Contours of Single Phase Gas Jet for Aspect Ratio 20 Nozzle at NTS 80

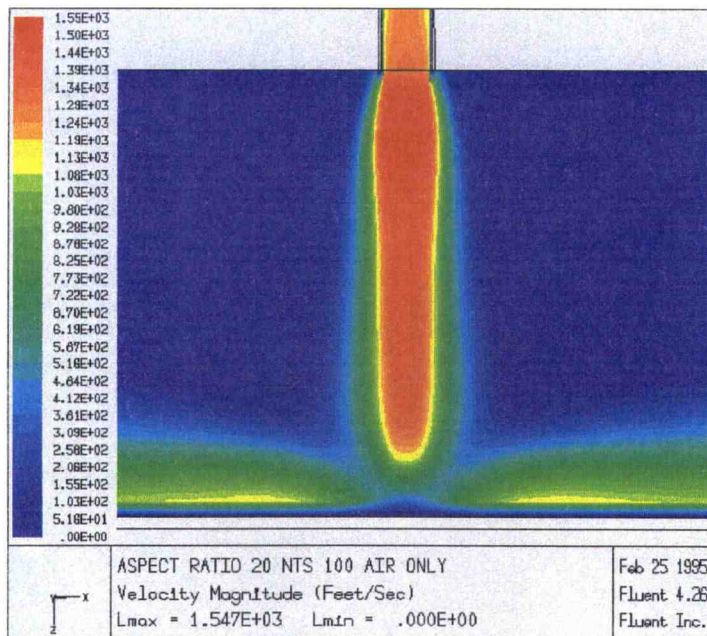


Figure 29: Velocity Contours of Single Phase Gas Jet for Aspect Ratio 20 Nozzle at NTS 100

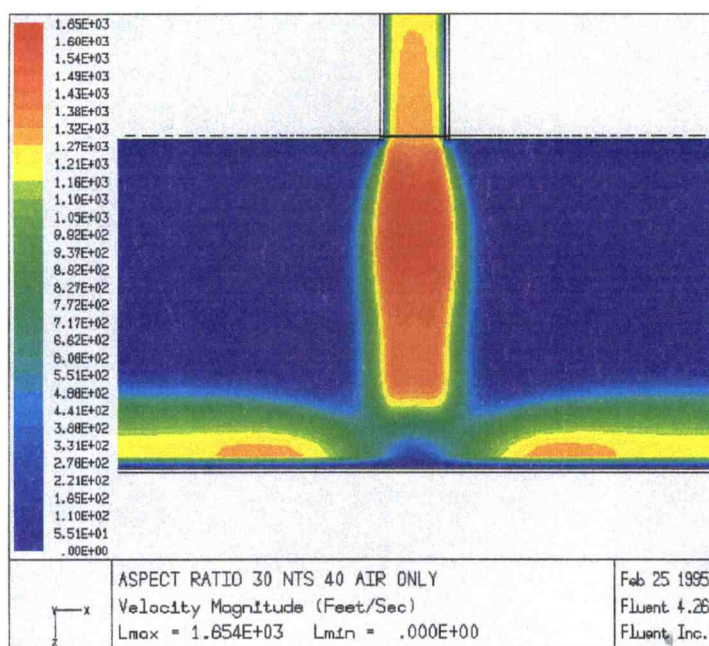


Figure 30: Velocity Contours of Single Phase Gas Jet for Aspect Ratio 30 Nozzle at NTS 40

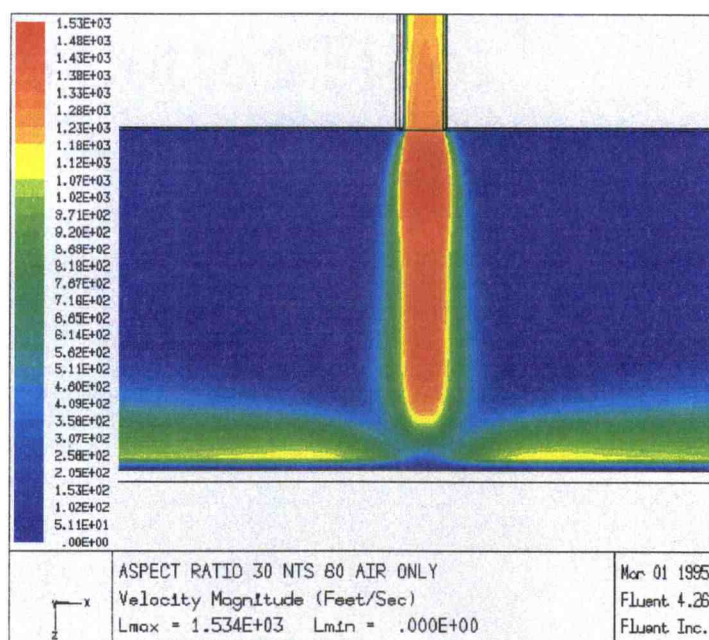


Figure 31: Velocity Contours of Single Phase Gas Jet for Aspect Ratio 30 Nozzle at NTS 60

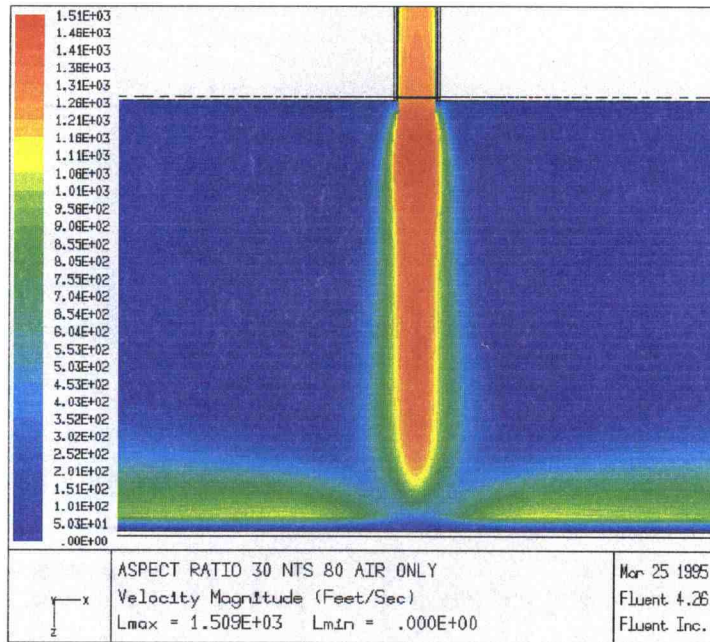


Figure 32: Velocity Contours of Single Phase Gas Jet for Aspect Ratio 30 Nozzle at NTS 80

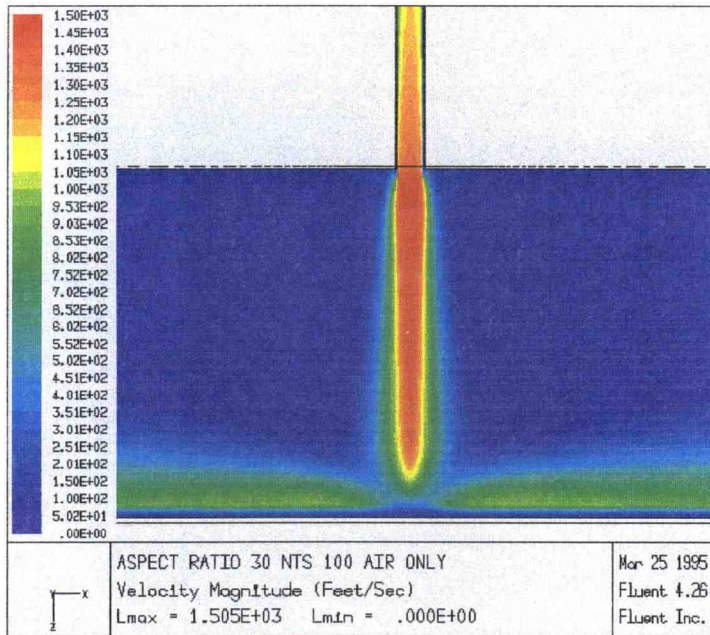


Figure 33: Velocity Contours of Single Phase Gas Jet for Aspect Ratio 30 Nozzle at NTS 100

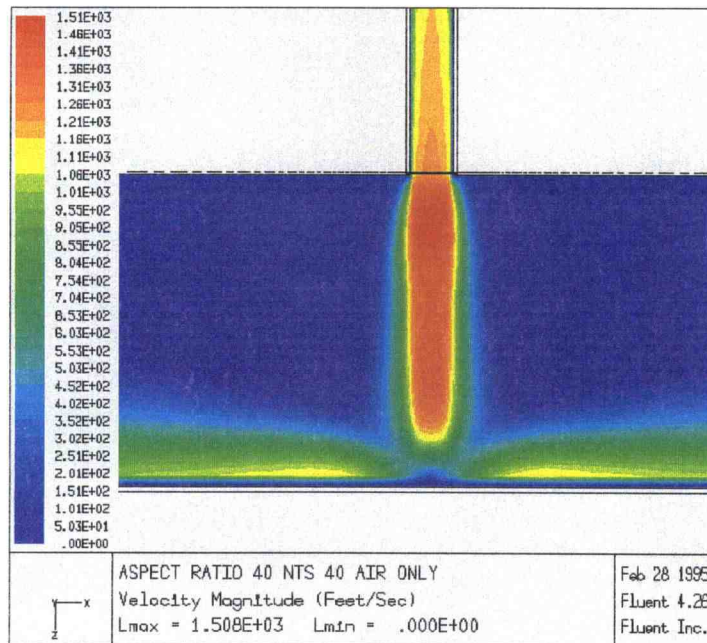


Figure 34: Velocity Contours of Single Phase Gas Jet for Aspect Ratio 40 Nozzle at NTS 40

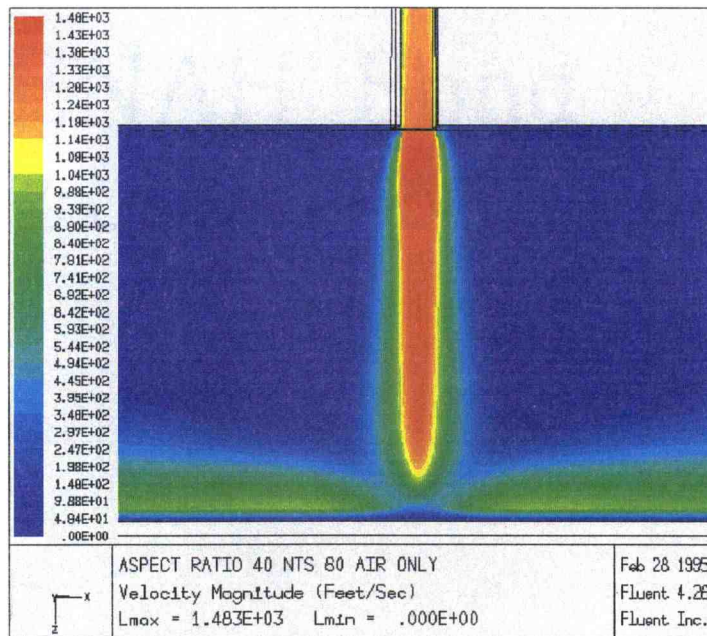


Figure 35: Velocity Contours of Single Phase Gas Jet for Aspect Ratio 40 Nozzle at NTS 60

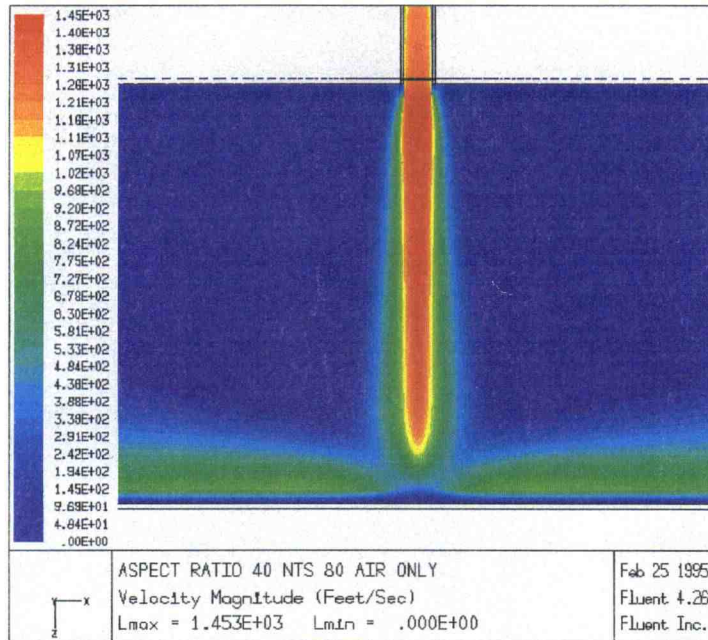


Figure 36: Velocity Contours of Single Phase Gas Jet for Aspect Ratio 40 Nozzle at NTS 80

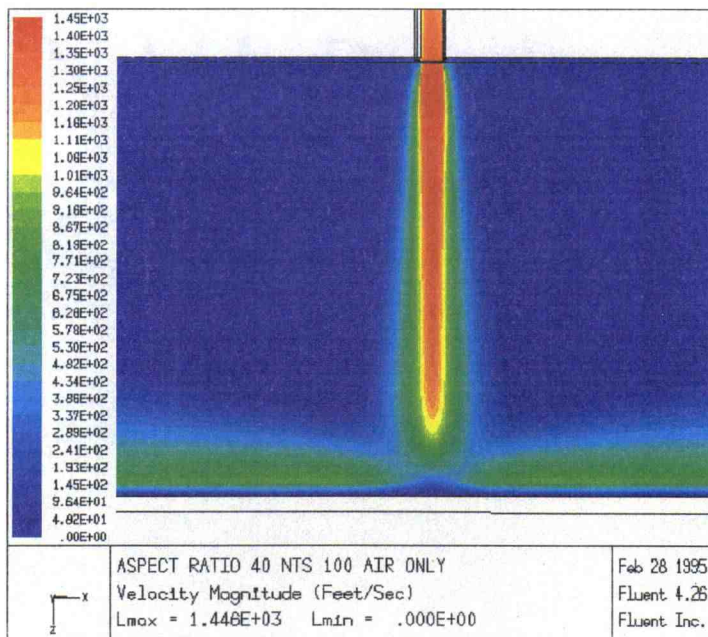


Figure 37: Velocity Contours of Single Phase Gas Jet for Aspect Ratio 40 Nozzle at NTS 100

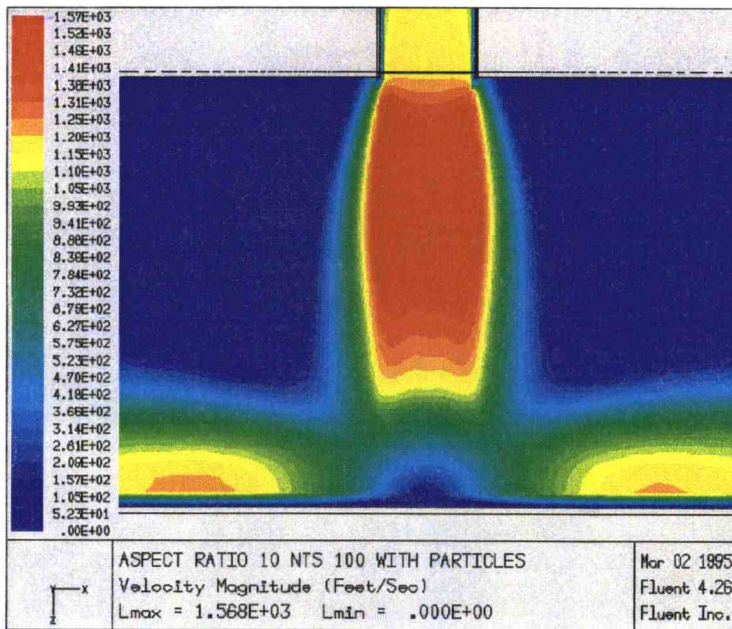


Figure 38: Velocity Contours of Two Phase Flow Jet for Aspect Ratio 10 Nozzle at NTS 100

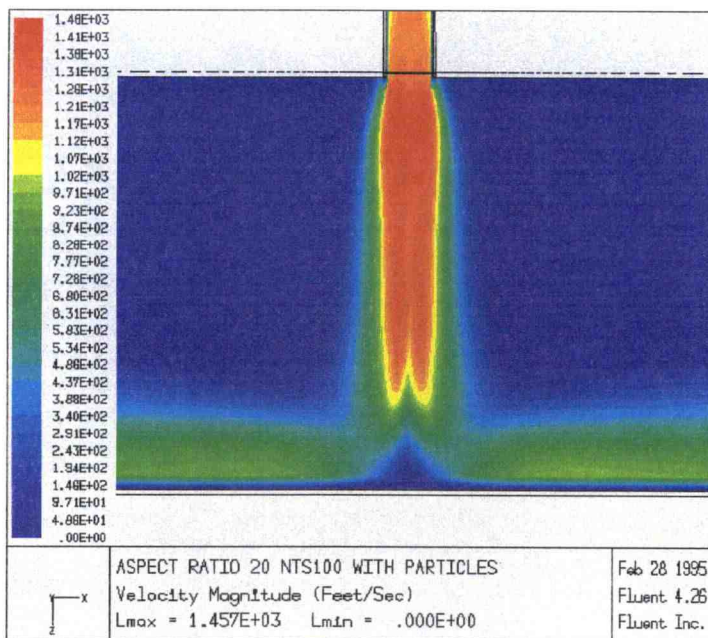


Figure 39: Velocity Contours of Two Phase Flow Jet for Aspect Ratio 20 Nozzle at NTS 100

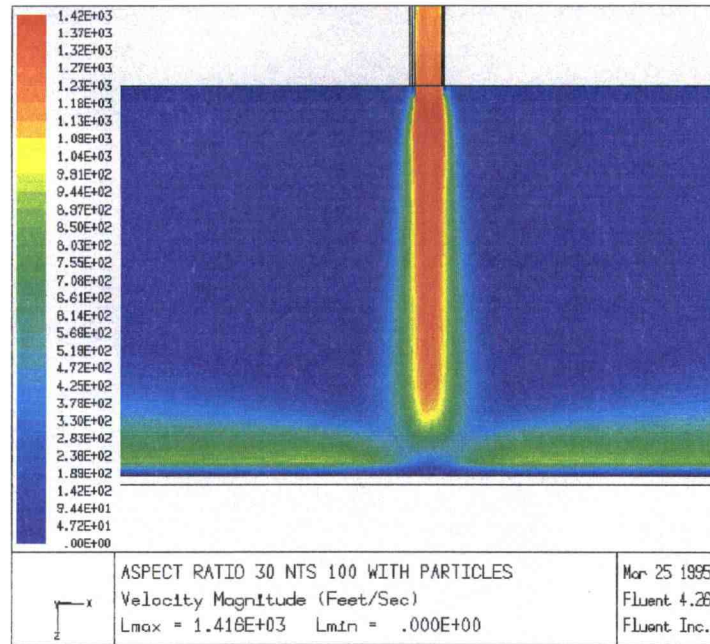


Figure 40: Velocity Contours of Two Phase Flow Jet for Aspect Ratio 30 Nozzle at NTS 100

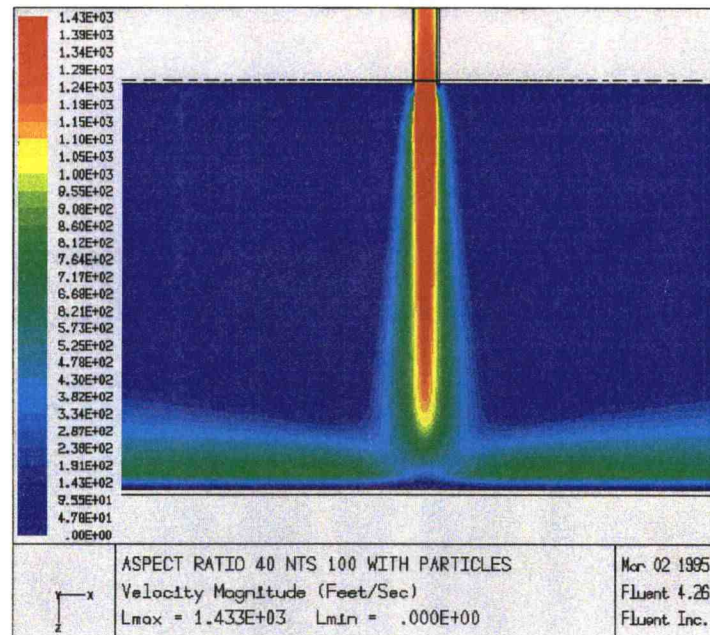


Figure 41: Velocity Contours of Two Phase Flow Jet for Aspect Ratio 40 Nozzle at NTS 100

Validation of FLUENT was accomplished first by comparing the mass flowrate of the gas through the nozzles at an inlet pressure of 80 psi. The results are tabulated in table 6. It can be seen that an average of only 12.0% error is presented by FLUENT.

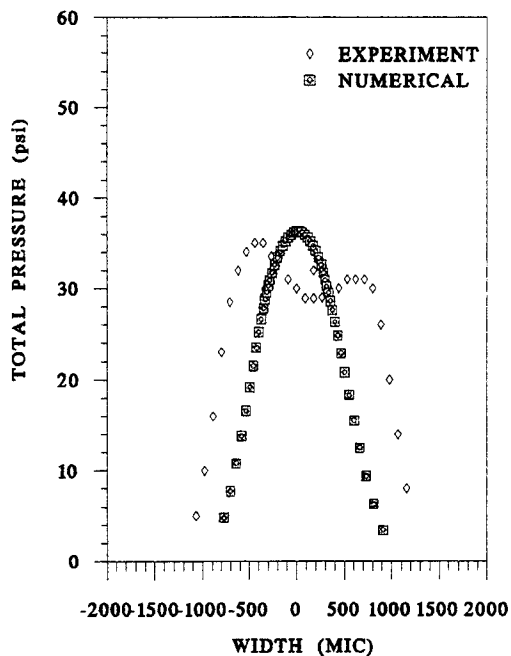
Table 6: Air Flowrate Comparison

Aspect Ratio	Air Flowrate Experimental (lbm/hr)	Air Flowrate Numerical (lbm/hr)	Percentage Error
10	28.11*	26.66	5.43
20	10.79	12.40	13.0
30	6.57	7.46	11.0
40	4.55	5.18	12.0

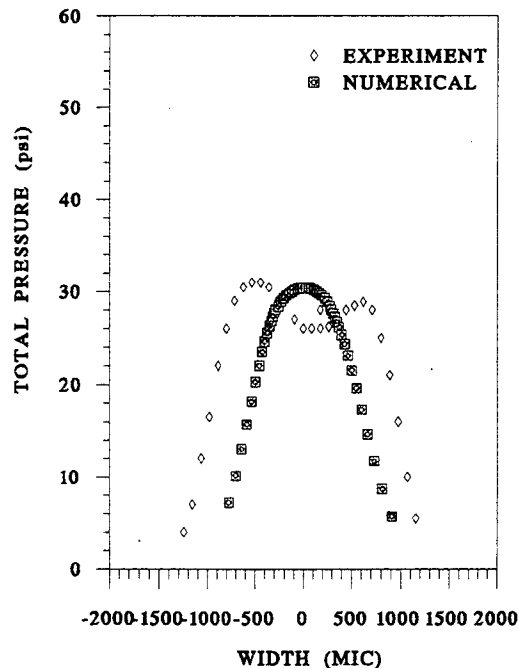
* Extrapolated mass flowrate; actual value exceeded instrument capability

The average error of 12 % was computed from aspect ratio 20, 30 and 40 nozzles only. Aspect ratio 10 nozzle was not used because the flowrate of this nozzle exceeded the maximum range of the mass flowrate meter. The mass flowrate of the air in the aspect ratio 10 nozzle was found by extrapolating from the largest reading measured by the mass flow meter. Figure 42a to 45d show the comparison of the

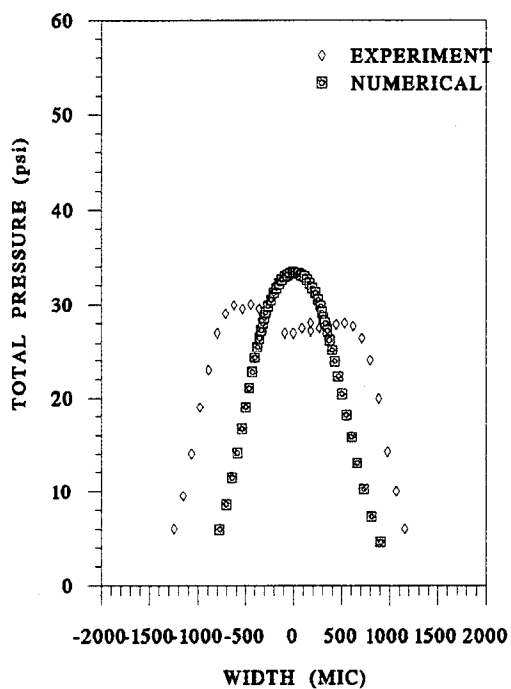
total pressure measured experimentally at the plate with the pressure from numerical simulation. The plots show that both results agree quite well with the only exception being that the plots obtained experimentally are broader. The double peak for aspect ratio 10 nozzle is due the strength of the jet. This phenomenon was also report by Krothapalli (1979 pg 336).



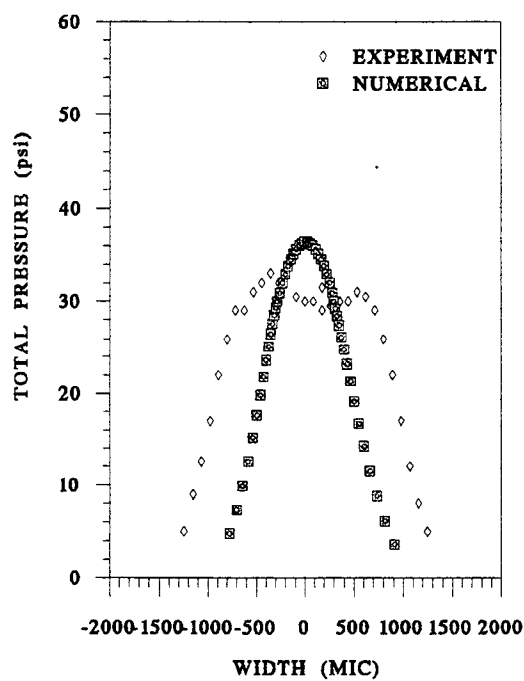
(a) NTS 40



(b) NTS 60

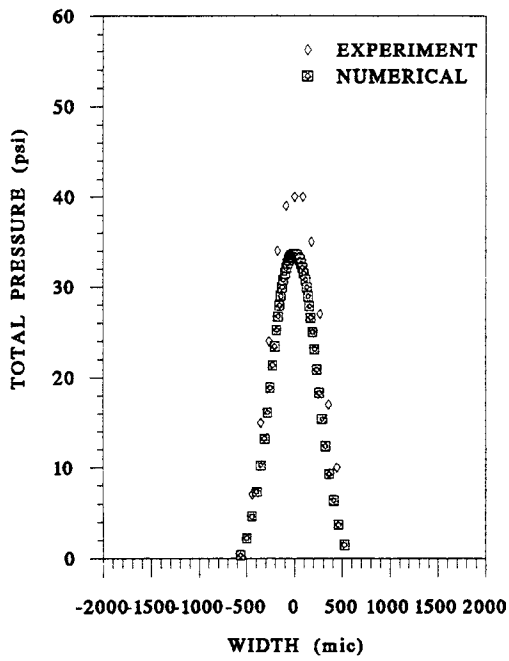


(c) NTS 80

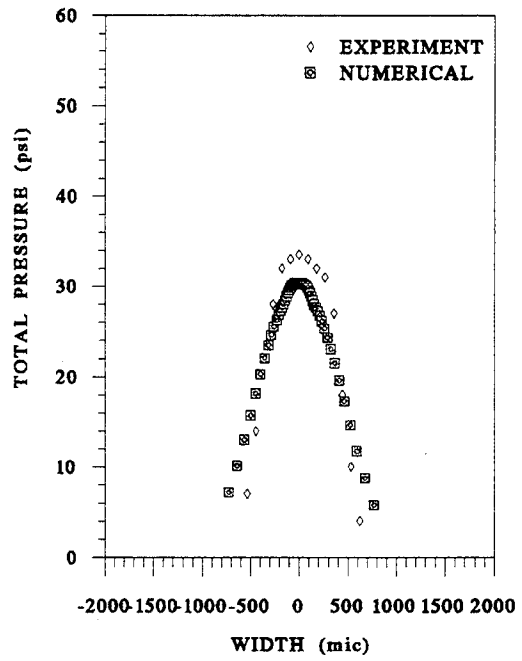


(d) NTS 100

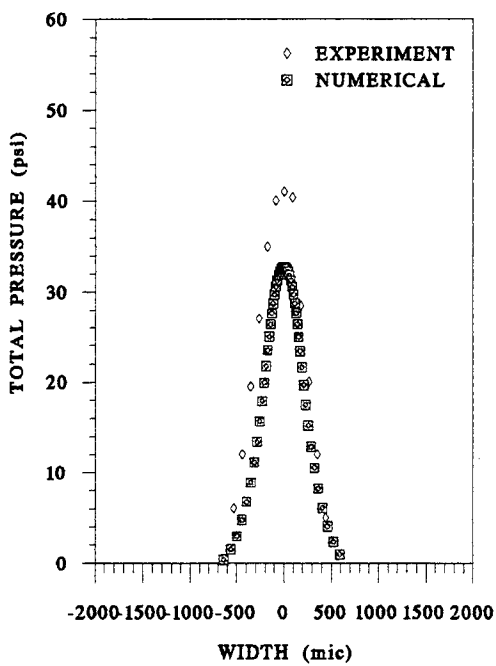
Figure 42a to 42d: Total Pressure Comparison for Aspect Ratio 10 Nozzle



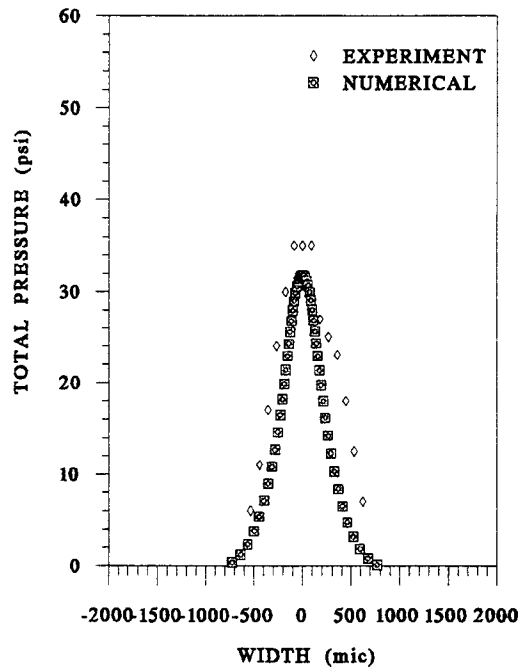
(a) NTS 40



(b) NTS 60

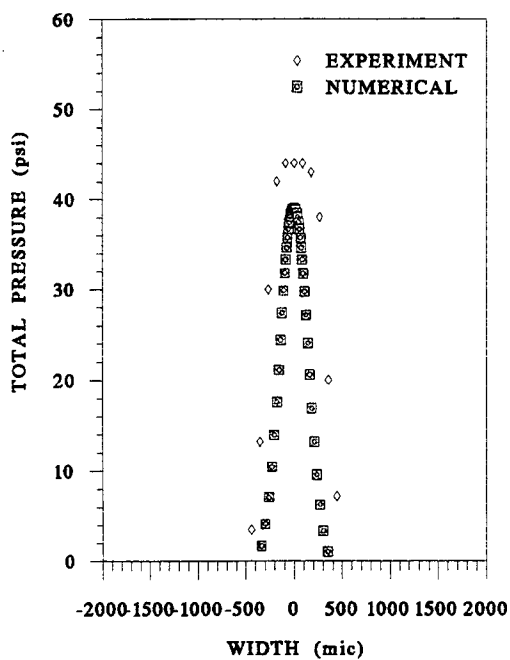


(c) NTS 80

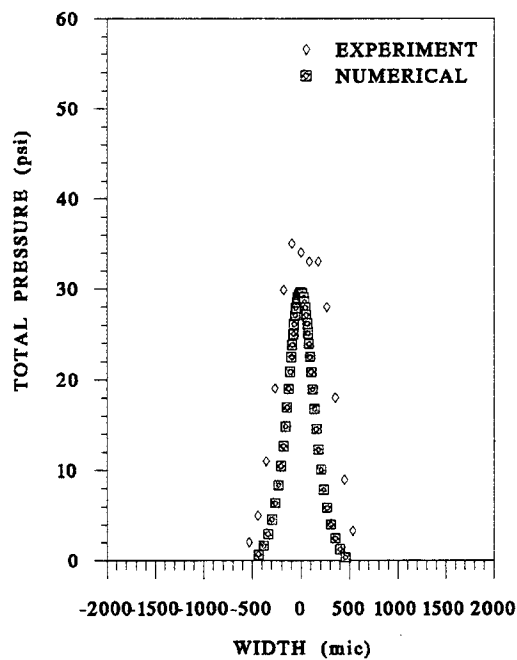


(d) NTS 100

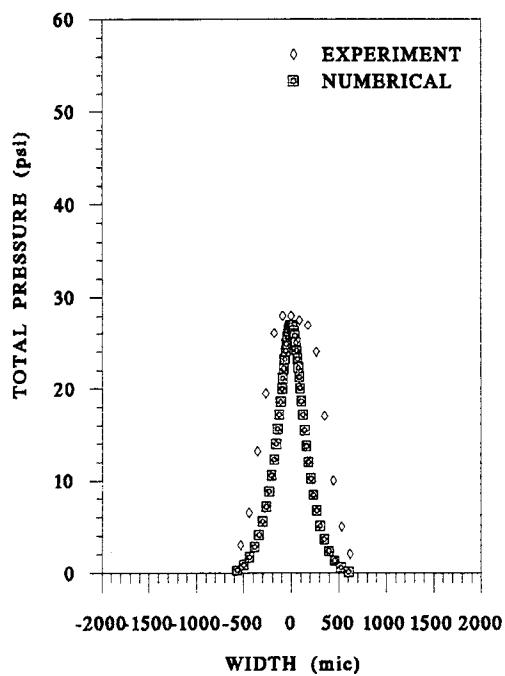
Figure 43a to 43d: Total Pressure Comparison for Aspect Ratio 20 Nozzle



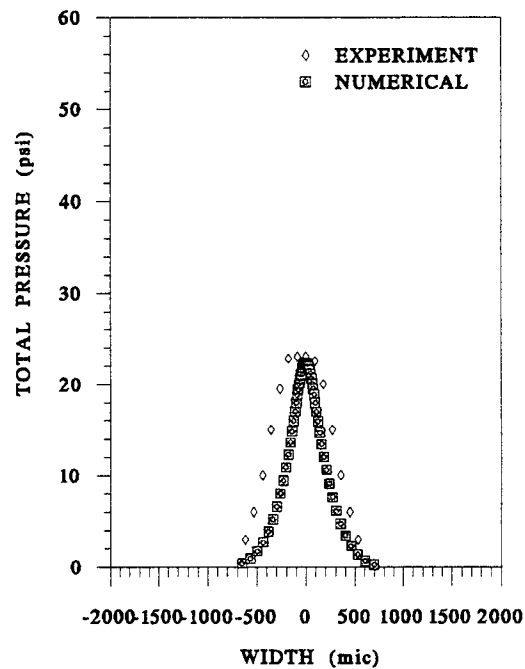
(a) NTS 40



(b) NTS 60

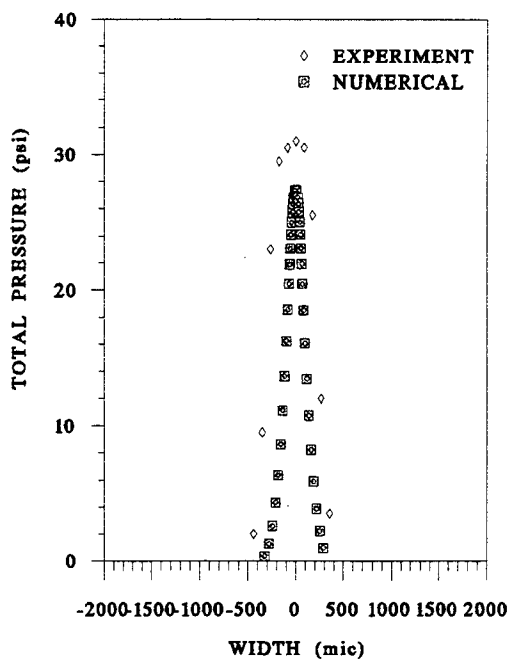


(c) NTS 80

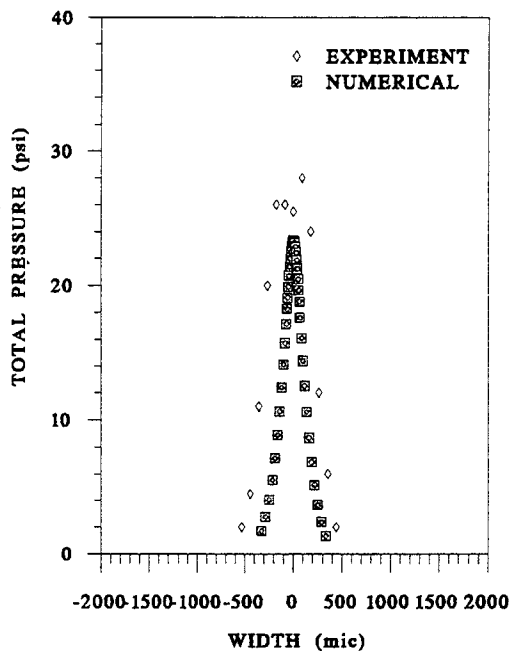


(d) NTS 100

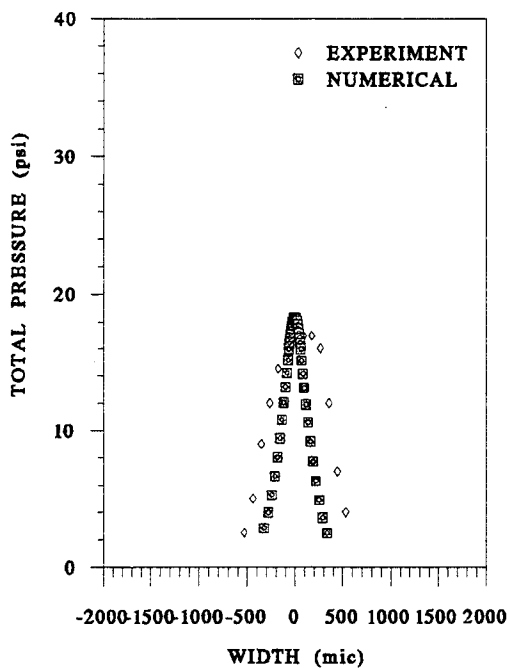
Figure 44a to 44d: Total Pressure Comparison for Aspect Ratio 30 Nozzle



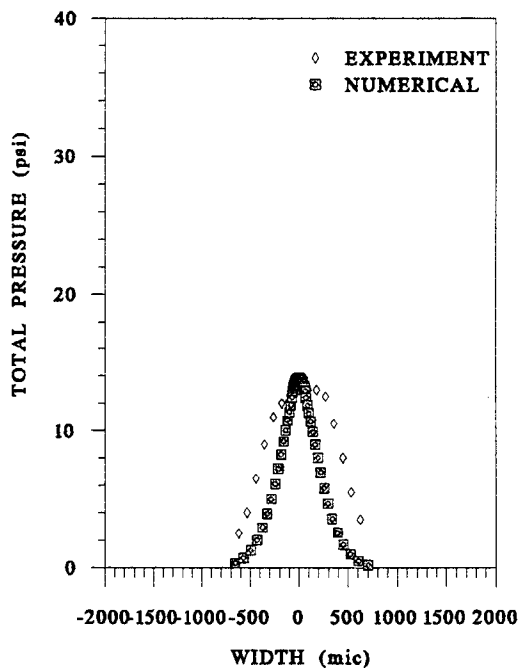
(a) NTS 40



(b) NTS 60

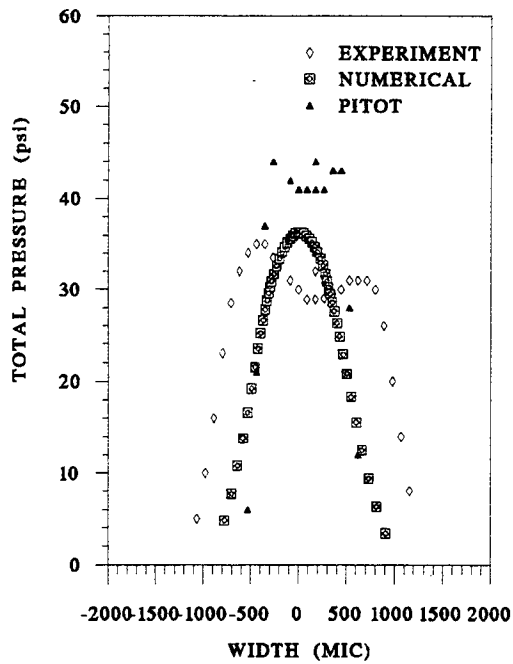


(c) NTS 80

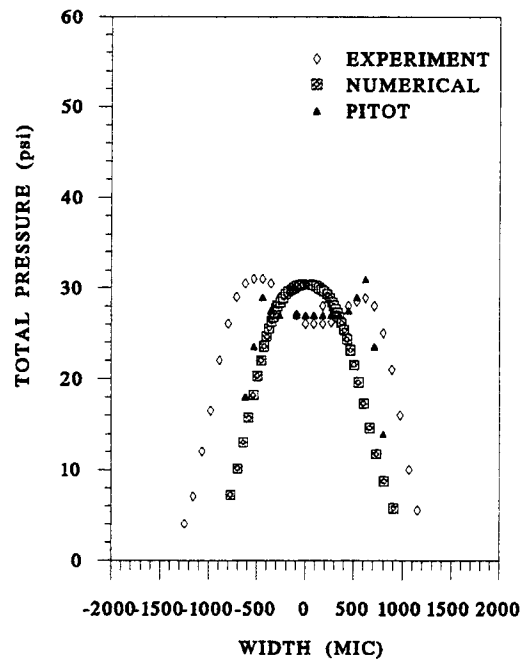


(d) NTS 100

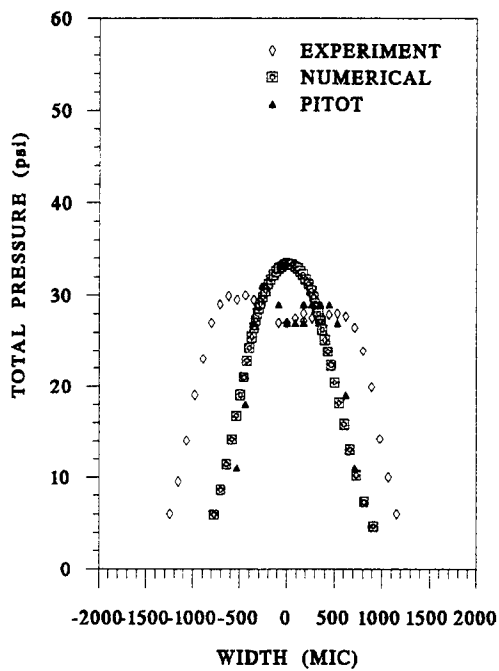
Figure 45a to 45d: Total Pressure Comparison for Aspect Ratio 40 Nozzle



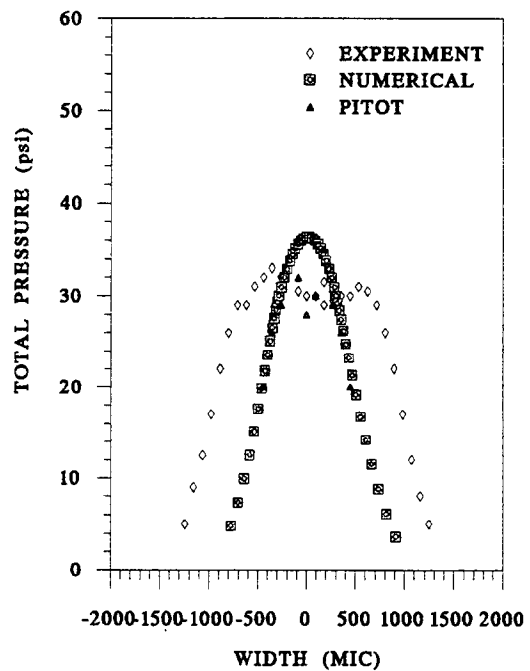
(a) NTS 40



(b) NTS 60



(c) NTS 80



(d) NTS 100

Figure 46a to 46d: Total Pressure Comparison Aspect Ratio 40 Nozzle with 0.006 inch Pitot tube

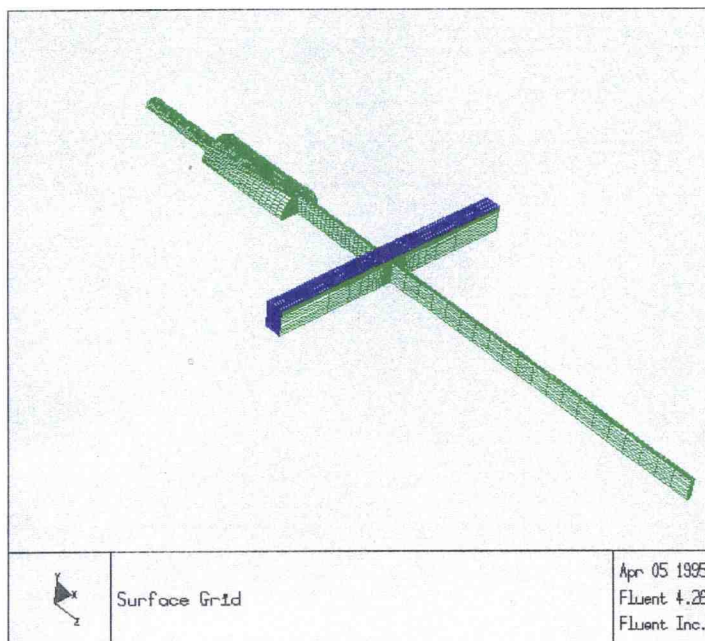


Figure 47: Geometrical Meshing of Model with Tube at the Plate to Simulate a Pitot Tube

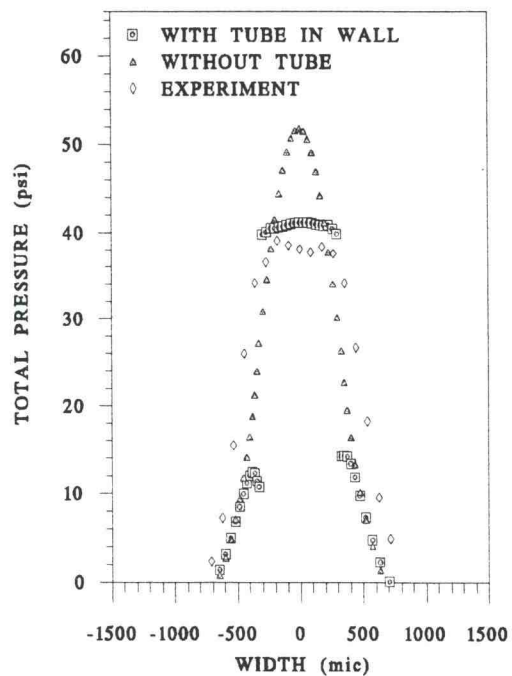


Figure 48: Pressure Plots Showing the Effect of Tube by Numerical Method

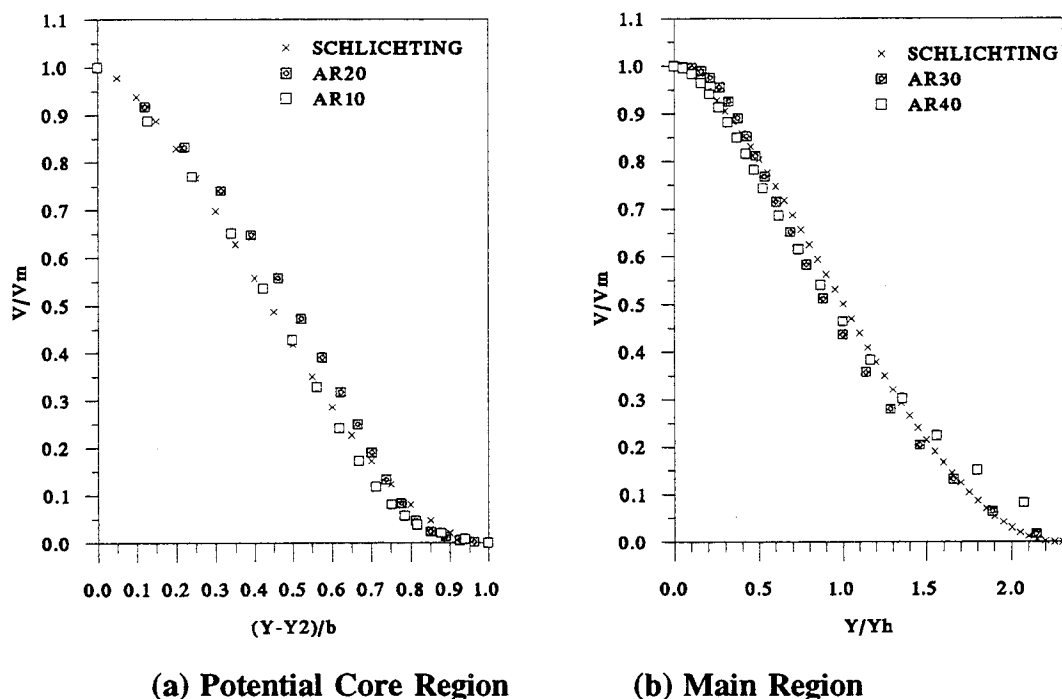


Figure 49a and 49b: Verification with "Schlichting Formula"

The wider plots are attributed to the interaction of the jet with the main air stream and the disturbances caused by the tube. The pitot tube used for the above measurement was of a 25 gauge tube. A new measurement for the aspect ratio 10 nozzle at all the NTS distances with a customized pitot tube of 0.006 inch in diameter shows better agreement in Figure 46a to Figure 46d. Unfortunately, measurements were not made for the other nozzles. This was because the pressure transducer was not sensitive enough to measure the pressure of other nozzles. In Figure 47, it shows the geometrical meshing of the model with a closed end tube to represent the pitot tube. The total pressure of this model was plotted and compared with pressure from a simulation without a tube and with the measured pressure. The plot in Figure 48

further substantiate that the 25 gauge tube had an adverse effect on the measurement.

The "Schlichting formula" was also used to check the results from the numerical method. The "Schlichting formula" and the plots from the numerical method are shown in Figure 49a and 49b and both graphs not only show good agreement but also show that the formula can be used to determine which region the abrasive jet is operating in. In this case, aspect ratio 10 and 20 nozzles were operating in the potential core whereas aspect ratio 30 and 40 were operating in the main region.

VALIDATION OF TWO PHASE FLOW

Validation of the two phase flow as stated before will be based on physical observation at this stage. Photographs showing the erosion of the nozzle are depicted in Figure 50a and 50b. The photographs show heavy erosion at the entrance of the nozzle and also at the wall just beyond the entrance. Plot of particle tracks obtained from numerical simulation is shown in Figure 51. The figure shows that many of the particles collided at the nozzle entrance and also many collisions occurred at the wall of the nozzle just beyond the entrance similar to the actual erosion seen in figure 50a and 50b.

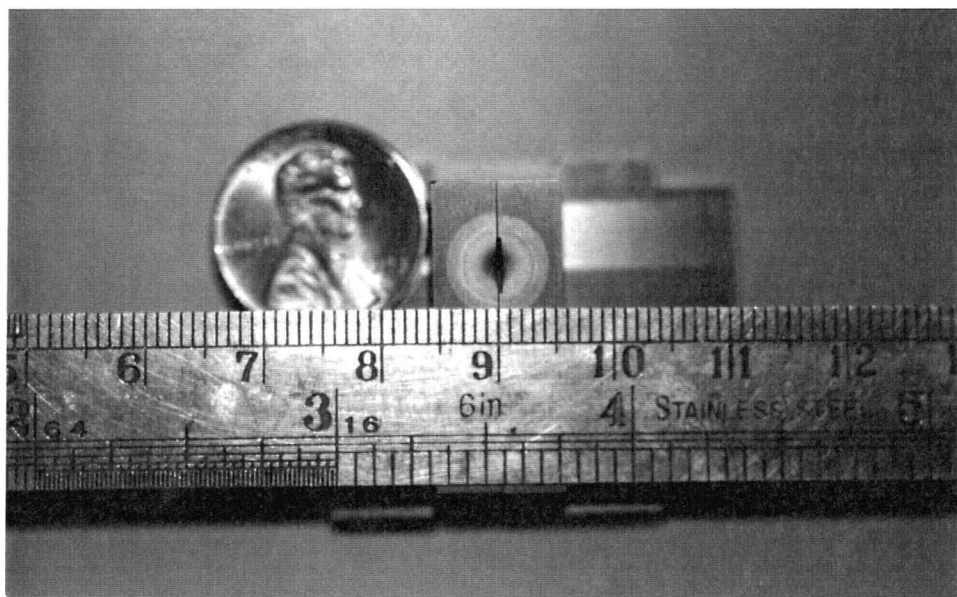


Figure 50a: Photograph Showing Erosion at the Entrance of Nozzle

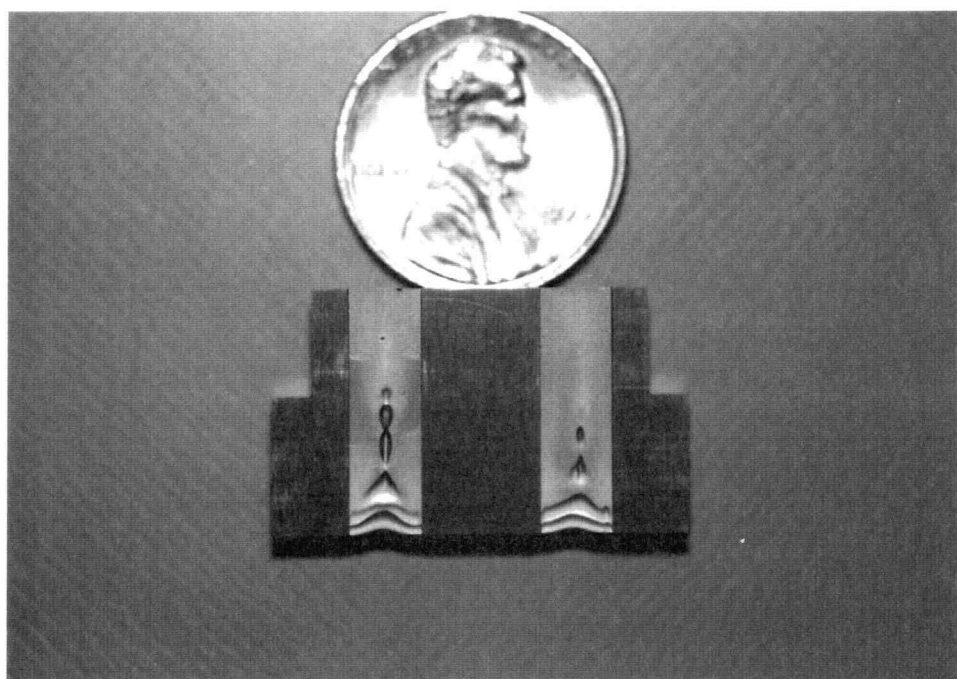


Figure 50b: Photograph Showing Erosion at Wall of Nozzle

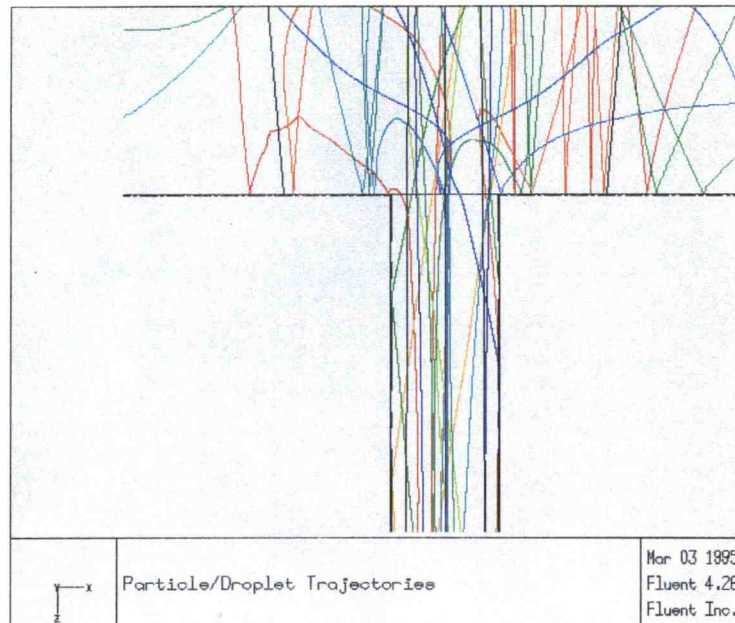
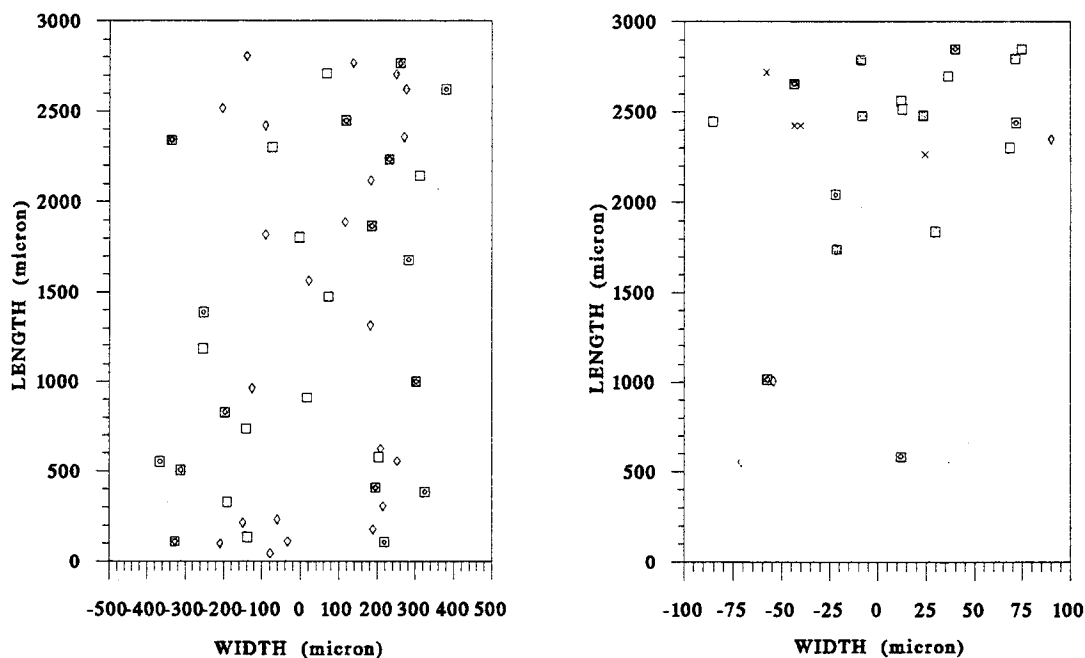


Figure 51: Particle Tracks Showing the Points of Impact at Nozzle Entrance and Wall

In correlating the momentum contour of the second phase jet at the point of impact to the contour of the drilled hole. The co - ordinates and velocity of each particle as it impinged onto the plate were extracted from FLUENT. Plots of the particle's positions for both aspect ratio 10 and 40 nozzles at an NTS distance of 100 mils, are shown in Figures 52a and 52b. The plots were divided into ten bins along the length, and frequency count were made. To obtain the energy contour of the impinging particle, an average momentum for each bin was calculated by multiplying the mass of each particle with its respective velocity within a bin. The momentum was then summed up and averaged by dividing by the total number of particles in the bin. The momentum was then normalized and plotted together with the normalized depth of the crater measured along its length. A half length plots of these energy and

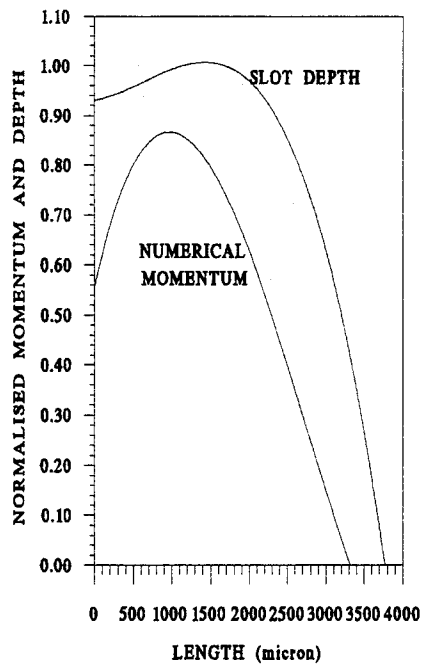
depth contours are shown in Figures 53a and 53b. These plots are only made to show the trends of the curves and not meant to be used as a basis for numerical comparison. This is due to the fact that the momentum plots of the impinging particles at the moment of impact does not include the drilling time, the coefficient of restitution and the properties of both the particles and the plate. There is no doubt that normalized depth curves represent the footprint of the particle jet energy which includes the factors of the dwelling time, properties of the particles, and properties of the plate all of which are contributing factors for calculating erosion rate.



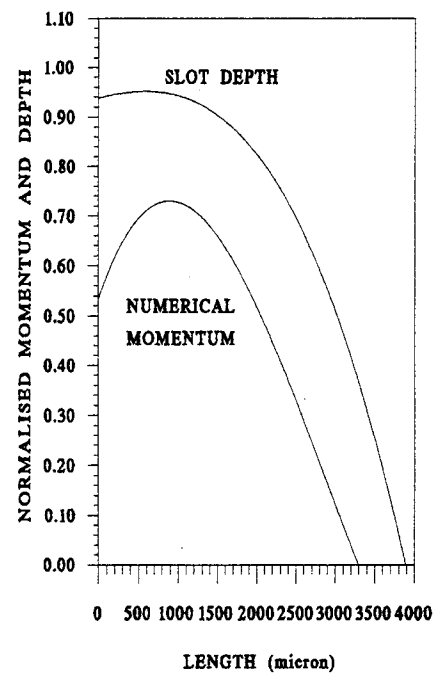
(a) Aspect Ratio 10 Nozzle

(b) Aspect Ratio 40 Nozzle

Figure 52a and 52b: Particle Impact Points on Steel Plate for Aspect Ratios 10 and 40 Nozzles at NTS 100 mils



(a) Aspect Ratio 10 Nozzle



(b) Aspect Ratio 40 Nozzle

Figure 53a and 53b: Normalized Momentum and Depth Comparison along Length of Slot

CONCLUSIONS

The overall goal of this project was to provide experimental data for the drilling rates of nozzles at various standoff distances of nozzle to substrate. A better understanding of the drilling behavior of a micro - rectangular nozzle will allow better designs and reduce overall time for designing nozzles. The end results of this are the production of better quality and more consistent rectangular hole for all nozzle sizes. In addition to the experiments, an attempt was made to correlate the numerical output contours of the momentum at the fluid and substrate interface, to the variation in the drilling rate or shape from a commercially available software package.

Data from the experiments revealed that the drilling rate depended on the standoff distance, operating pressure, and the mixture ratio. Maximum penetration values were obtained at different NTS distances and pressures. In an aspect ratio 10 nozzle a maximum penetration of 35 microns was found at a standoff distance of 40 mils with an inlet pressure of 120 psi (see figure 19a). Maximum drilling depth of 50 microns for an aspect ratio 20 nozzle was found to be at a standoff distance of 80 and 100 mils at inlet pressure of 100 and 120 psi respectively. At a pressure of 105 psi, an aspect ratio 30 nozzle has the greatest drilling depth of 85 microns at an NTS distance of 40 mils. In an aspect ratio 40 nozzle a penetration depth of 125 microns occurred at the standoff distance of 60 mils with nozzle inlet pressure of 120 psi

It appears from the experiments that more attention needs to be paid to the change of the width rather than to the length when designing the nozzle. This is

because the width seems to be more sensitive to the change of the parameters that influence the drilling operation. Although linear trends were produced for the growth of the width and length, more needs to be done to establish the trend for NTS distances and mixing ratio.

Numerical simulations were first performed for the single phase and this solutions were used as an initial condition to solve for the second phase solution. Experiments for the gas phase were conducted to verify the simulated results. The validation showed that the numerical results agree well with the experimental results; i.e. total pressure and air mass flowrate. However, second phase verification was not possible at this time due to the absence of appropriate instruments in measuring the momentum of the abrasive particles and at the same time, FLUENT is not able to produce the momentum contour of the second phase directly at a specified cur-plane. As a result an indirect approach was used as an attempt to relate the momentum of the jet to the profile of the crater. This was done by assuming that the profile of the rectangular crater was the signature of the two phase jet imprinted onto the plate. With the position, size, and velocity of each particle extracted from FLUENT text file , normalized momentum plots were drawn and calculated. Good behavioral agreement was shown when comparison of these graphs with normalized plots of the depth of the crater measured along the length.

This tedious approach was resorted to because the project's area of interest was too specialized i.e. momentum contours of the particles phase and in addition, FLUENT is a general purpose code therefore the post processing capability were not

sophisticated enough for this project. However, it will not be justifiable at this point in time to draw a conclusion that FLUENT was not suitable for this project. Instead it was felt that FLUENT was under-utilized because it has a capability for a user to use a "USER SUBROUTINE" function to write a special code to suit its needs. In the case of this project the "USER SUBROUTINE " function was not explored. Apart from this limitation, FLUENT was able to assist the nozzle designer by showing the area where the nozzle erosion was the greatest and the path taken by the particles. This indeed can help the nozzle designer spot the short comings of the nozzle before it is released for production.

BIBLIOGRAPHY

- Balanin, B.A., Lashkov, V.A., and Trakhov, YE.P., ''*Aerodynamic Drag in Two-Phase Flows*'', Fluid Mechanics, Soviet Research, vol. 10, No. 1, Jan-Feb 1981.
- Balanin, B.A., and Zlobin, V.V., "*Effect of Inserts on the Shaping of Fine-Particle Conveying Flows in Cylindrical Nozzles*", Fluid Mechanics, Soviet Research, vol.10, No. 1, Jan-Feb 1981.
- Bhattacharya, A., "*New Technology*", The Institution of Engineers (India), 1977, p.32.
- Bitter, J.G.A., "*A Study of Erosion Phenomena Part I*", Wear, vol.;6, 1963, p.5.
- Ch. Wulf, and W. Konig, "*The Influence of the Cutting Parameters on Jet Forces and the Geometry of the Kerf*", Seventh Intl. Symp. on Jet Cutting Technology, June 26th - 28th, 1984
- Finnie, I., "*Some Observations on the Erosion of Ductile Metals*", Wear, vol.19, 1972, p.81.
- Finnie, I., "*Erosion of Surface by Solid Particles*", Wear, vol. 3, 1960, p.87.
- Fisher, M.A., and Davis, F.E., "*Study on Fly Ash Erosion*", Mech. Engg., vol.71, no.6, 1949, p.481.
- Forthmann, E., "*The Theory of Turbulent Jet by Abramovich. G.N ., p 7.*", 1963. The M.I.T. Press, Massachusetts institute of Technology, Cambridge, Massachusetts.
- Hatta, N., Fujimoto, H.,and Ishii, R., "*Numerical Analysis of a Gas-Particle Subsonic Jet Impinging on a Flat Plate*", ISIJ INTL, Vol. 31 No.4 pp 342-349, 1991.
- Ingulli, C.N., "*Abrasive Jet Machining*", Tool and Manufacturing Engineers, vol.9, no.5, 1967, p.28.
- Kinoshita, T., "*An Investigation on the Compressible Properties of Liquid-Jet and Its Impact on to the Rock Surface*", Third Intl. Symp. on Jet Cutting Technology, 11th-13th May 1976, Chicago U.S.A.
- Krothapalli, A., Baganoff, D., and Karamcheti, K., "*Turbulence Measurements in a Rectangular Jet*", AIAA 17th Aerospace Sciences Meeting, Jan 15-17, 1979 New Orleans, La.

Marster, G.F., "*The Effects of Upstream Nozzle Shaping on Incompressible Turbulent Flows from Rectangular Nozzles*", Transactions of the CSME, vol 5, No. 4 1978-79

Marster, G.F., "*An Experimental Investigation of Spanwise Velocity Distributions in Jets from Rectangular Slots*", AIAA 18th Aerospace Sciences Meeting, Jan 14-16, 1980 Pasadena, California.

Sheldon, G.L., and Finnie, I., "*The Mechanism of Material Removal in the Erosive Cutting of Brittle Materials*", J of Engg. for Ind. Trans. ASME Series B, vol.88, 1966, p.393

Smeltzer, C.E., Gulden, M.E., and Compton, W.A., "*Mechanism of Metal Removal by Impacting Dust Particle*", J. of Basic Engg. Trans. ASME, vol.92, 1970, p.639.

Sommerfeld, M., "*Experimental And Numerical Studies on Particle Laden Underexpanded Free Jets*", Gas-Solid Flows . ASME Feb, vol. 121, 1991.

Tilly, G.P., "*Erosion Caused by Impact of Solid Particles*", in Treatise on Materials Science and Technology, vol. 13, edited by D. Scott, Academic, New York, 1979, p 287-319.

Verma, A.P. and Lal, G.K., "*An Experimental Study of Abrasive Jet Machining*", Intl. Jl. Mach.Tool. Des. Res., 1984, 24, No. 1, 19-2.